SAPIENZA
UNIVERSITÀ DI ROMA

Optimization of the Onboard Processing for Data Volume Reduction in SAR Systems

Facoltà di Ingegneria Civile e Industriale

Corso di Laurea Magistrale in Ingegneria Spaziale e Astronautica

Anastasia Schilirò

Relatore
Prof. Pierfrancesco Lombardo

Correlatore
Dr. Michelangelo Villano (DLR)

A.A. 2018-2019

Acknowledgements

This thesis is the results of six months of research activity at the Microwave and Radar Institute of the German Aerospace Center (DLR) in Oberpfaffenhofen, Germany. I would like to express my appreciation and thanks to my supervisor Dr. Michelangelo Villano for his wise guide and the professionalism shown during my internship. Moreover, I would also like to thank my advisor Prof. Pierfrancesco Lombardo for the opportunity given to me and the wonderful experience. Another thanks go to my colleagues, in which I have found friends before working partners. Last but not least I would like to express my deepest gratitude to my parents who have always believed in me, to whom this thesis is dedicated.

Oberpfaffenhofen, July 2019

Anastasia Schilirò

Contents

1 Introduction

Synthetic aperture radar (SAR) is a remote sensing technique, capable of providing high-resolution images independently of weather conditions and sunlight illumination. The Synthetic Aperture Radar (SAR) principle was discovered by Wiley in 1951. Wiley suggested that high angular resolution could be achieved by analyzing the spectrum of the receiving signal from a coherent radar system. In 1953, the University of Michigan's developed the first airborne SAR. Enormous technological development in the following years led to the realization of a SAR system on board satellite SEASAT, that was launched in 1978. Since that time, many SARs have flown on board the Space Shuttle and SAR was developed more extensively and numerous satellites for Earth observation. Table 1 shows some missions that were developed in the years for Shuttle missions, satellite and airborne.

Tab. 1 Some SAR Systems

	Sensor	**Year**	**Resolution**	**Band**	**Agency/Country**
Shuttle missions	SIR-A	1981	40 m × 40 m	L	NASA/USA
	SIR-B	1984	25 m × 17 m	L	NASA/USA
	SIR-C	1994	10 m ×30 m	L, C, X	NASA/USA
	X-SAR/SRTM	2000	25 m × 25 m	C, X	NASA, DLR, ASI
Satellite	SEASAT-SAR	1978	25 m x 25 m	L	NASA/USA
	ERS-1	1991	26 m × 28 m	C	ESA
	ALMAZ-1	1991	15 m × 20 m	S	USSR
	RADARSAT	1995	10 m × 9 m	C	CSA/Canada
	ENVISAT	2002	25 m × 25 m	C	ESA
	ALOS-PALSAR	2006	9 m x 10 m	L	JAXA/Japan
	Cosmo-SkyMed	2007	1 m x 1 m	X	ASI/Italy
	TerraSAR-X	2007	1 m x 1 m	X	DLR/Germany
	TanDEM-X	2009	1 m x 1 m	X	DLR/Germany
	RISAT-1	2012	3 m x 3 m	C	ISRO/India
	HJ-1-C	2012	5 m x 20 m	S	China
Airborne	PAMIR	2003	10 cm × 10 cm	X	Germany
	MISAR	2003	0.5 m × 0.5 m	Ka	EADS
	RAMSES	1994	10 cm × 10 cm	P,L,S,C,X,Ku,Ka	ONERA
	E-SAR	1994	1.5 m × 1.5 m	P,L,S,C,X	DLR

1.1 Spaceborne SAR Systems

The SAR sensors permit to obtain high resolution image for different applications:

- topography
- agriculture
- oceanography
- snow and ice monitoring (Fig. 1)
- environment monitoring
- volcano monitoring (Fig. 2)
- climate change monitoring
- hydrology (Fig. 3)
- traffic monitoring
- forestry (Fig. 4)
- etc.

In the last years, Earth remote sensing applications most often require sensors that permit continuous global coverage with high resolution image. The conventional SAR system cannot have at the same time, high resolution with wide-swath. Different techniques have been proposed to overcome this limitation. In this thesis will be given attention to the Staggered SAR that permits to have at the same time width wide coverage and high resolution HRWS using digital beamforming DBF techniques.

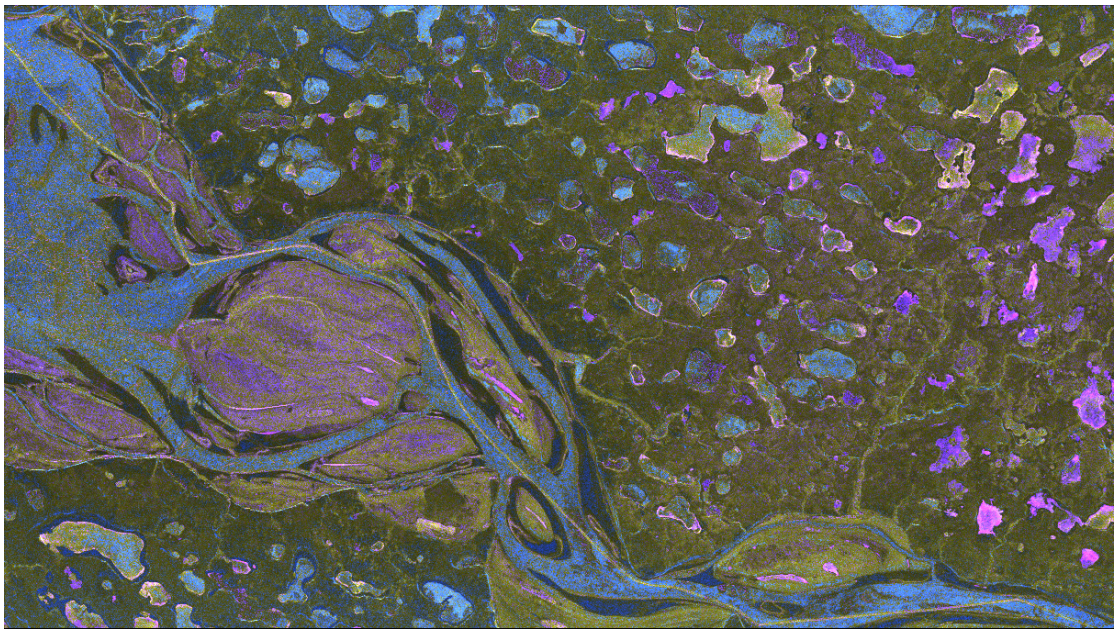

Fig.1 Image from TerraSAR-X satellite. The image shows layers of snow and ice that cover the Mackenzie River in Canada [1].

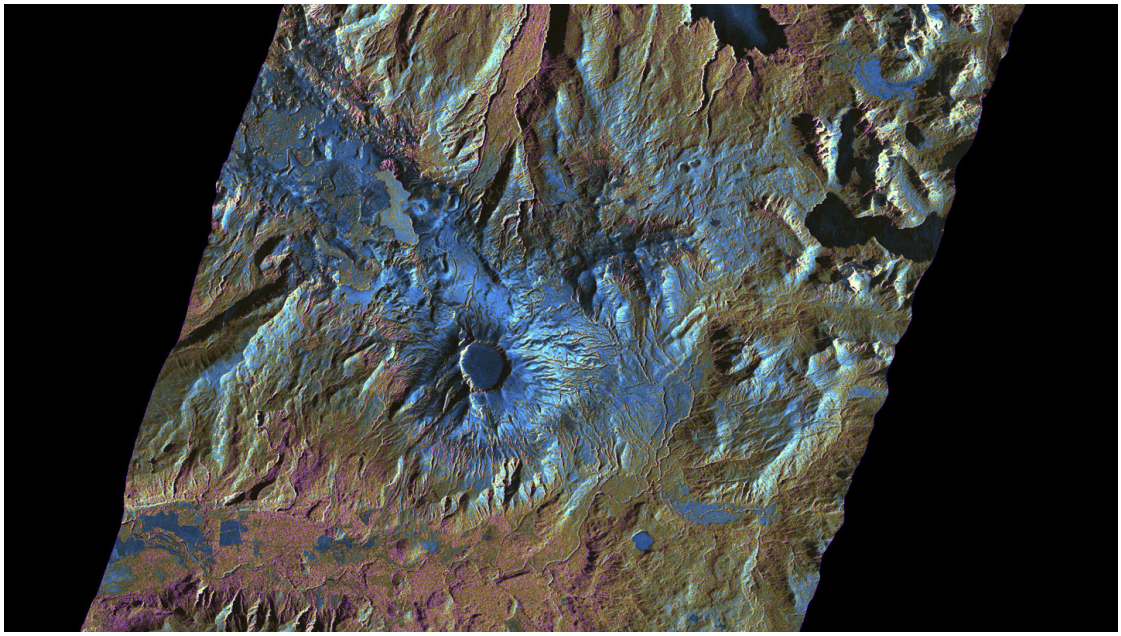

Fig. 2 The Puyehue-Cordón Caulle volcano region on 6 July 2011. The light blue colored area is the lava field that has formed to the west of the new crater [1].

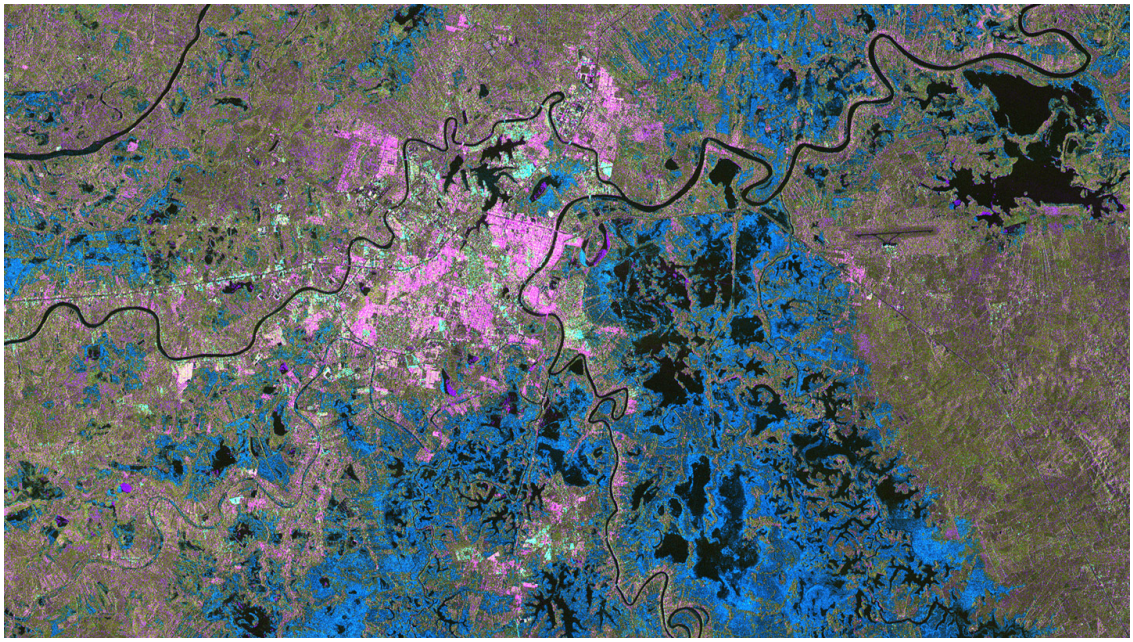

Fig. 3 Image of flooding in Mexico obtained in November 2007[1].

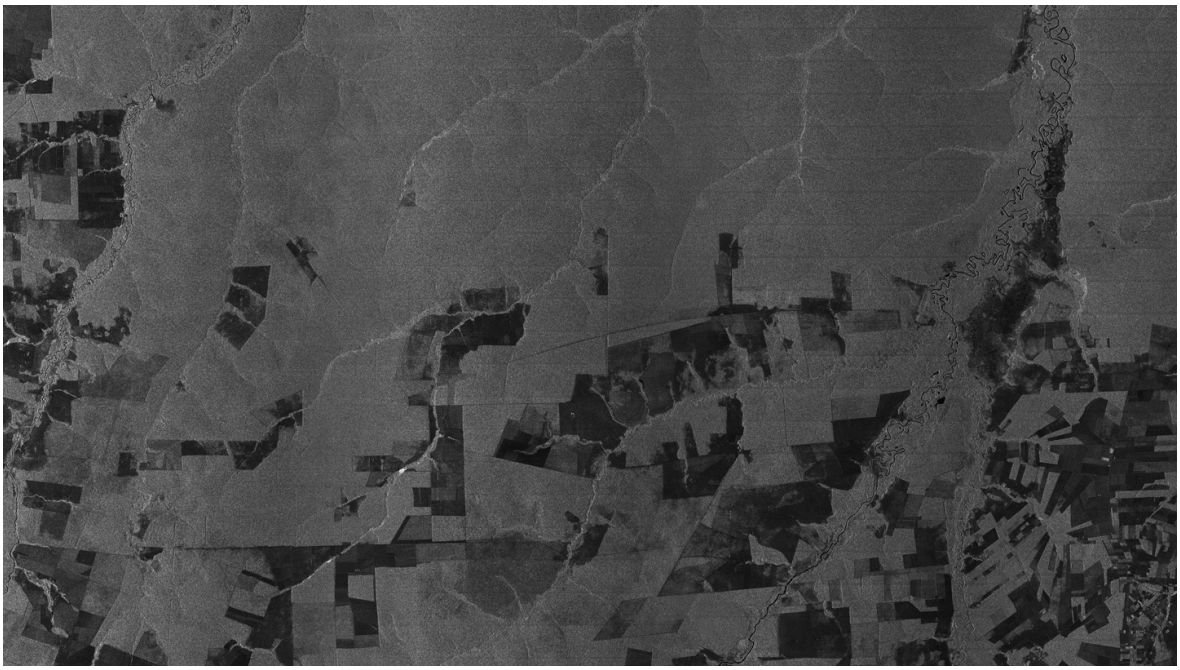

Fig. 4 Mato Grosso, Brazil. The north of the province is dominated by the fringes of the Amazon rainforest where logging has been particularly extensive in recent years [1].

The coming years, according to current planning, could be launched a satellite with high resolution-wide swath called Tandem L (Fig. 5). Tandem-L mission is based on global observation with high resolution.

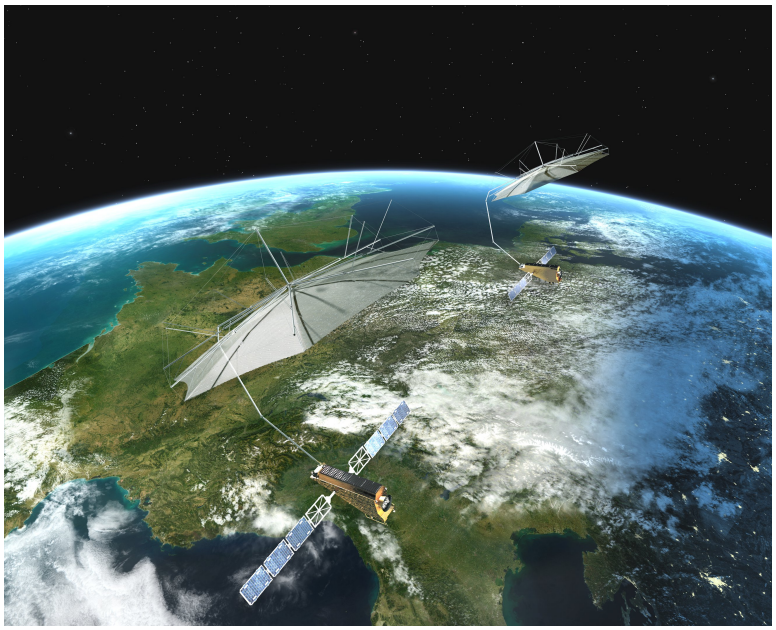

Fig. 5 Tandem-L satellites [3].

Tandem-L will provide information in the areas of the biosphere, geosphere, cryosphere and hydrosphere. The big advance of Tandem-L is that allows global coverage in 8 days with 350 km

swath [2], compared, for example with TanDEM X that requires one year to achieve global coverage and the swath is 30 km.

Tandem-L will give a better understanding of the Earth system and its dynamics.

1.2 Motivation, Objectives, and Structure of the Thesis

In recent years the interest of SAR research is increasingly shifting to the issues of SAR High Resolution Wide Swath (HRWS). The HWRS SAR permits to reach a global coverage in some days, compared with the conventional SAR that to reach a global coverage it needs more or less one year.

To improve the performance of HRWS has been proposed the Staggered SAR technique. The staggered SAR technique permits to reduce "blind ranges" that are present between the different subswaths and obtains a wide continuous swath. The idea consists of the continuous variation of the pulse repetition interval (PRI) between consecutively transmitted pulse [4]. Together with an average oversampling in azimuth allows interpolation of non-uniformly sampled raw-data on a uniform grid.

Staggered SAR is a promising solution to image wide swaths without gaps based on digital beamforming.

All this improvement of performance of conventional SAR systems required a huge amount of data volume. In according with huge data, is required on board processing that permits to reduce the amount of data before to transmit to the ground. Staggered SAR requires high azimuth oversampling.

In according with limited memory it is necessary to make on-board processing and reduce the data volume before the downlink. The challenging task that requires new processing techniques to permit the downlink and stores the data on satellite.

In this thesis it will be considered two algorithms that permit to reduce data volume onboard satellite. The first algorithm permits to reduce data volume before the downlink but do not consider the limited memory of Field Programmable Gate Array (FPGA) on board satellite. The second algorithm is a suboptimal strategy that considers the limited memory of FPGA considering a limited number of samples (taps).

In this thesis the processing performance of suboptimal algorithm based on limited numbers of taps with single and quad polarization and for different margin bandwidth will be analyzed.

Thanks to performance analysis different parameters it will be esteemed in order to achieve an optimal compromise.

The thesis is structured as follows. Section 2 provides a short review of satellite SAR, including the description of the signal processing and an overview of the principal parameters of a SAR system. Section 3 describes high-resolution wide swath and Staggered SAR and the relative amount of data volume. To reduce the "blind ranges" between the subswath it is done an interpolation and oversampling in azimuth that corresponds to high value of PRF [4]. Unlike the high value of PRF corresponds a huge amount of data and for this reason it is necessary to take into account onboard processing.

It is considered a strategy to reduce data volume on board satellite before the downlink. Section 4 describes a new strategy that permits to reduce the data volume on board with a limited number of taps and reduce in this way the memory of FPGA. In section 5 analysis it will perform several parameters in order to achieve an optimal compromise and find the best strategy to be applied to the suboptimal case. Finally, conclusions are drawn in Section 6, where an outlook for further research is also provided.

2. State of Art: Spaceborne SAR Systems

SAR systems are designed to produce high spatial resolution microwave images. The functioning of the SAR is based on the fact that the radar antenna, mounted on satellite or on airplane, moves with a certain velocity. Whenever it emits the Radio Frequency (RF) pulse (usually a chirp) and receives its echo, it is in a different position due to the motion of the platform. If all these echoes relating to different instants are collected and memorized, it can be thought that they derive from a different portion of the same antenna, with larger dimensions of a real aperture radar. By appropriately processing these echoes it is possible to reconstruct what would have been the return signal of the long antenna.

Synthetic Aperture Radars were developed as a means of overcoming the limitations of real aperture radars. These systems achieve good azimuth resolution that it is independent of the slant range to the target, yet use small antennas and relatively long wavelengths to do it.

Microwaves can penetrate through clouds, vegetation and soil, and can operate in day and or night conditions. Also, the Radars are sensitivity to dielectric properties this allows for example to distinguish liquid and frozen water.

Consider a satellite with constant speed v_s in a straight line at constant height h_s. The dimensions of the antenna are the length L and height W. The direction of travel of the platform is known as azimuth direction or along-track and direction perpendicular to the radar's flight path is slant range[4].
The antenna emits pulses of electromagnetic energy with a constant pulse repetition frequency (PRF). The return echoes arrive at the antenna at different times, depending on the distance from the antenna to the specific scattering object on the ground.

The area illuminated by the radar beam in the ground is given by equation (1)

$$W_g = \frac{\lambda R_0}{W \cos \eta} \tag{1}$$

where R_0 is slant range, η is the incidence angle and $\lambda = \frac{c_0}{f_0}$ is the radar wavelength. The synthetic aperture length is given by:

$$L_s = \frac{\lambda R_0}{L} \tag{2}$$

The azimuth resolution for a SAR is:

$$\delta_a = R_0\theta = R_0\frac{\lambda}{2L_s} = \frac{L}{2} \tag{3}$$

the factor 2 appears because of the two-way path from the transmission to reception. The equation (3) suggests that a short antenna yields a fine azimuth resolution. In Fig. 6 is shows SAR geometry, Swath Width, Ground Range, Slant Range and Azimuth Direction.

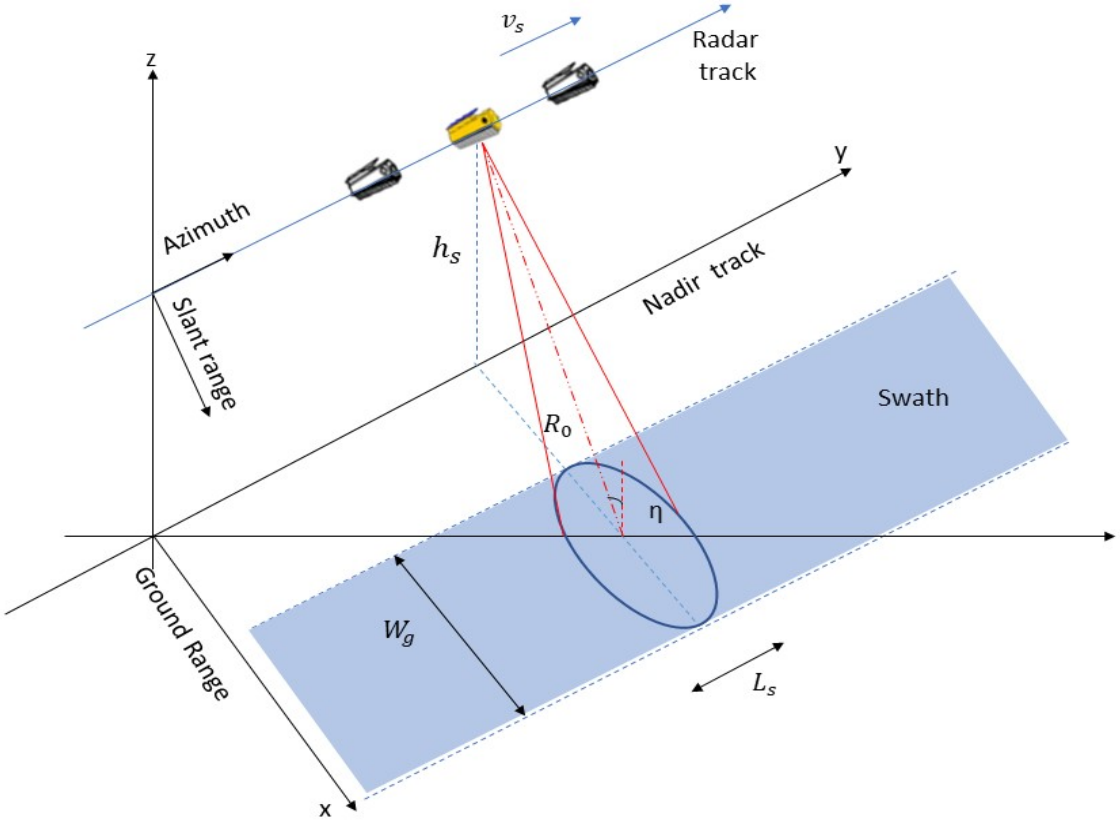

Fig. 6 Simplified geometry of a SAR.

2.1 Signal Processing

The main goal of SAR data processing is the determination of the range and azimuth coordinates of the targets lying in the strip-map to obtaining a focused SAR image. The image that is obtained from SAR is raw and should be processed to obtain a focused image. Each complex sample of the received echo signal is given by its real and imaginary part. The received echo signal data form a two-dimensional matrix with coordinates time delay and pulse number. Time delay corresponds to slant range and pulse number to the azimuth.

The processing could be considered as two separate matched filter operations along the range and azimuth dimensions. The most common algorithm employed in most of SAR processing system is a two-dimensional correlating procedure. The two dimensions of the correlation processing are realized as two one-dimensional matched filter operations namely range compression and azimuth compression as shown in Fig. 7 where range compressed data are obtained from the convolution with reference function, and azimuth compressed data are obtained with the convolution of azimuth reference function that is variable with the range. The first matched filtering operates on the single pulse radar returns and the second matched filtering operation operates on the Doppler signal.

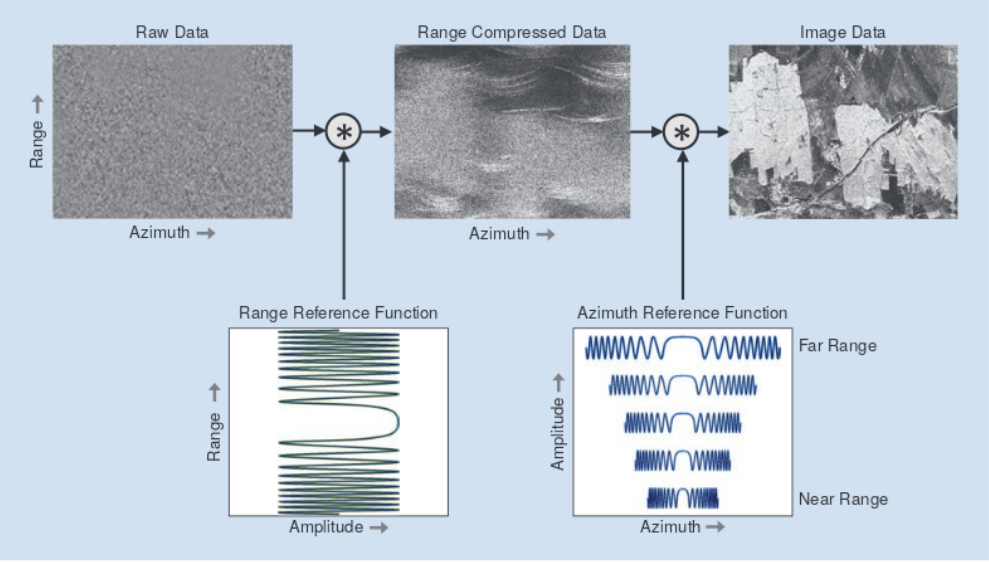

Fig. 7 SAR processing steps, where the range of compressed data result from a convolution of the raw data with the range reference function. In a second step the azimuth compression is performed through convolution with the azimuth reference function [5].

2.1.1. Range Compression

Let us consider $s(t)$ the transmitted signal after modulation by the radar antenna and $r(t)$ the received signal after coherent demodulation.

$$r(t)=As(t-\frac{2R_0}{c_0})\exp(-j\frac{4\pi R_0}{\lambda})+n(t) \tag{4}$$

The relation (4) takes in account of a delayed, attenuated, shifted version of s(t), white Gaussian noise $n(t)$ and A the attenuation. The range processor starts with the range compression as a rule as "fast correlation" performed in the range frequency domain.

The matched filter is used for compression due to maximizes the output signal-to-noise ratio (SNR). The matched filter is linear and time invariant and the corresponding impulse response is given by

$$h(t)=s^*(-t) \tag{5}$$

The output y(t) of the matched filter for a rectangular input waveform

$$s(t)=rect(\frac{1}{\tau})=\begin{cases}1, & |t|\le\tau/2\\ 0, & |t|>\tau/2\end{cases} \tag{6}$$

is given by

$$y(t)=\begin{cases}\tau(1-\frac{|t|}{\tau}), & |t|\le\tau\\ 0, & otherwise\end{cases} \tag{7}$$

this result is obtained from the convolution of rectangular input for the corresponding complex conjugation. The output response is a triangular waveform. The slant range approximately had the same form and it is multiplied to half speed of light in free space c_0 .

$$\delta R\simeq c_0\frac{\tau}{2} \tag{8}$$

From that equation (8) is deduced that for short pulse τ corresponds to higher resolution. At the same time for higher resolution corresponds a poor SNR and low radiated energy after matched filtering. To overcome this problem, many radar systems adopt a linear frequency-modulated (LFM), as known as "chirp":

$$s(t)=\exp(j\pi B\frac{t^2}{\tau})rect(\frac{t}{\tau}) \tag{9}$$

where B is the chirp bandwidth. The chirp is characterized by a constant amplitude and quadratic phase variation across the pulse profile. The output $y(t)$ of the matched filter is:

$$y(t)\simeq\tau sinc(B\tau) \tag{10}$$

where $sinc(t)$ is the cardinal sine:

$$sinc(t)=\frac{\sin(\pi t)}{\pi t} \tag{11}$$

the slant range resolution δR after chirp compression is given by the reciprocal of the chirp bandwidth B:

$$\delta R\simeq\frac{c_0}{2B} \tag{12}$$

2.1.2. Azimuth Compression

After range compression, the data is transformed into the azimuth frequency domain via FFT. In this case, the chirp is spontaneously generated by the relative motion of the sensor with the respect to the surface that is begin observed. The azimuth compression is done with a chirp in the domain of Doppler frequency.

$$f_D=\frac{2v_s\sin\varphi}{\lambda}\simeq\frac{2v_s x}{\lambda R_0} \tag{13}$$

Where φ is azimuth angle and x is the azimuth coordinate of the scatterer.

The azimuth resolution is given by:

$$\delta x\simeq\frac{\lambda R_0}{2v_s}\delta f_D=\frac{\lambda R_0}{2v_s}\frac{1}{T}=\frac{\lambda R_0}{2v_s}\frac{v_s L}{\lambda R_0}=\frac{L}{2} \tag{14}$$

the best attainable azimuth resolution is half the antenna length L.

The received signal $c(x)$ from a point-like scatterer when the platform moves along azimuth coordinate x and under the assumption of a rectangular antenna pattern in azimuth is given by

$$c(x)=\exp(-j4\frac{\pi R(x)}{\lambda})rect(\frac{x}{L_s}) \tag{15}$$

where $R(x)$

$$R(x)=\sqrt{R_0^2+x^2}\simeq R_0+\frac{x^2}{2R_0} \tag{16}$$

the output $v(x)$ after matched filter is

$$v(x)\simeq sinc(\frac{2L_s}{\lambda R_0}x)=sinc(\frac{2}{L}x) \tag{17}$$

the azimuth resolution δx can be expressed as a function of the Doppler bandwidth as

$$\delta x\simeq\frac{v_s}{B_D} \tag{18}$$

The result of the compression in azimuth and range is the obtaining of a data matrix that has on the columns the cells solved in distance and on the rows the cells solved in azimuth. Every element of the matrix is a complex number which is known the amplitude and the phase.

With range compression arises the problem of cell migration. The migration in range is the difference between the maximum distance, when a scatterer enters or leaves the antenna, and the minimum distance when the scatterer is at a minimum distance on the antenna axis. If the migration in range is a multiple of the range resolution there is one overlapping of data from one row to the other. To overcome this problem there are several algorithms that permit to reduce the observation time.

2.2 Single- and Quad-Polarization

A radar antenna is designed to transmit and receive electromagnetic waves with well-defined polarization. The polarization is defined as the orientation of the electric field vector in the plane orthogonal to the wave propagation direction.

A polarimetric radar can be designed to operate as a single-pol system, where there is a single polarization transmitted and a single polarization received. A typical single-pol system would transmit horizontally or vertically polarized waveforms and receive the same (giving HH or VV). A quad-pol or full-pol system would alternate between transmitting H- and V-polarized waveforms and receive both H and V (giving HH, HV, VH, VV) [6]. In a coherent system, the quad- pol measures 4 elements of the complex scattering matrix.

$$S = \begin{pmatrix} S_{HH} & S_{HV} \\ S_{VH} & S_{VV} \end{pmatrix} \tag{19}$$

By varying the polarization of the transmitted signal, SAR systems can provide information on the polarimetric properties of the observed surface such as land, ice, snow, ocean, and urban applications.

3. High-Resolution Wide-Swath Imaging

A SAR system is capable of providing high-resolution images. This makes SAR very attractive for the observation of the Earth's surface. However, the SAR system is limited to acquire images with both high-resolution and wide-swath coverage. The azimuth resolution (14) is inversely proportional to Doppler bandwidth and PRF (pulse repetition frequency):

$$\delta x \approx \frac{L}{2} \approx \frac{v_s}{B_D} \geq \frac{v_s}{PRF} \tag{20}$$

that results from a long synthetic aperture which is illuminated by a short antenna of length L. High resolution in azimuth needs a high value of B_D and high PRF. On the other hand, to guarantee an image with a wide width range W_g on the ground, it is required a low PRF:

$$W_g < \frac{c}{2 \cdot PRF \cdot \sin \eta} \tag{21}$$

Wide coverage can therefore be achieved only at the expense of a degraded azimuth resolution [10]. This limitation can be overcome using digital beamforming (DBF) techniques on receive techniques based on multiple receive subapertures (Fig. 8).

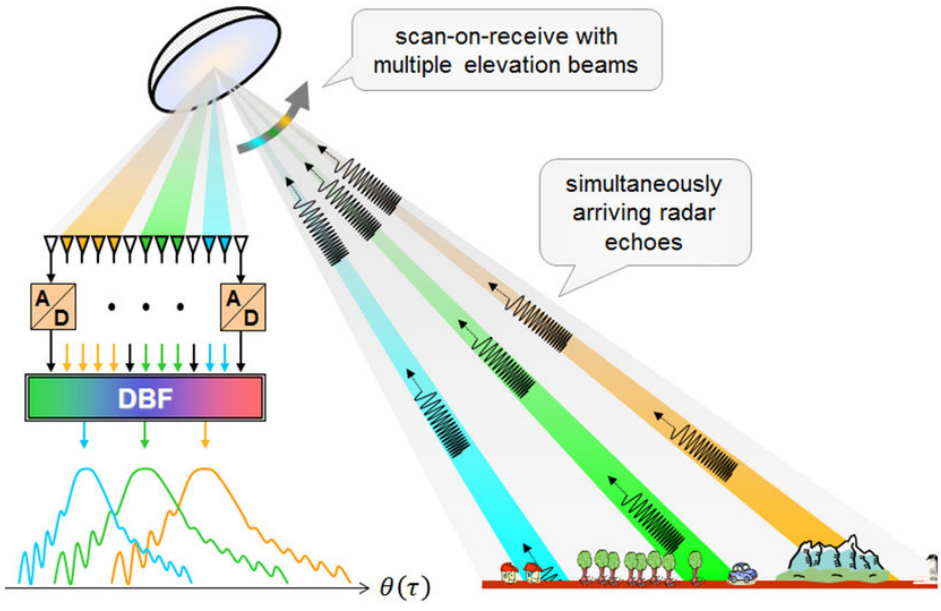

Fig. 8 Reflector SAR with multiple elevation beams. Digital beamforming on receive plays a crucial role in the reliable separation of the simultaneously arriving radar echoes from range-ambiguous positions [7].

In other words, the receive antenna is split into multiple sub-apertures. The signal received by each subaperture is individually amplified and digitized. The systems that employ a DBF technique improve SNR and suppress the range ambiguities. The name "digital beamforming" derives from the fact that it is performed by software. The advance of this technique permits to achieve simultaneous imaging on multiple subswaths through multiple elevation beams. There are different solutions for high-resolution wide-swath SAR imaging like: multiple beam SAR, high-resolution wide-swath (HRWS) SAR, multi-Channel ScanSar and HRWS SAR employing a reflector antenna [8]. This thesis will be focused on HRWS, in particular Staggered SAR.

3.1 Staggered SAR

The DBF technique has a limitation related to the blind range across the swath in particular are present between adjacent subswaths. The blind ranges are the consequence of periodical transmission of pulses, i.e., it is not possible simultaneously to receive and transmit the signal. After compression in azimuth, the image is characterized by discontinuous mapping, in particular the width in slant range $\Delta R_{0\ \text{blind}}$ of blind range is given by

$$\Delta R_{0\,\text{blind}} = c_0 \tau \qquad (22)$$

where τ is the duration of interval.

This problem is common in conventional SAR, characterized by uniform PRI, where blind ranges remain unchanged along the azimuth. A new strategy "Staggered SAR", discovered by DLR [8], resolve the problem of blind ranges changing continually PRI. The fig.9 shows the distribution of blind range for SAR with constant PRI and Staggered SAR.

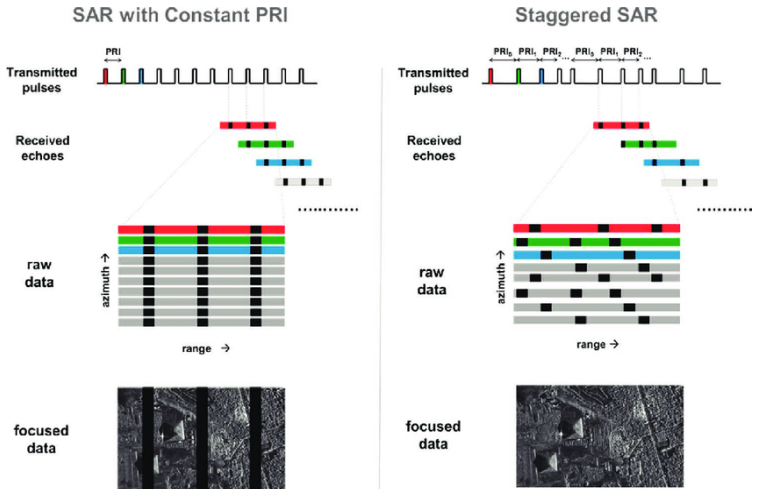

Fig. 9 Comparison conventional SAR and Staggered SAR [9].

The advance of changing continually PRI is that the blind range changes position for each transmitted pulse. Applying the interpolation it is possible to reconstruct the missing pulses and obtain a uniform grid, in this way only some of the transmitted sample is missing.

The processing strategies are based on the different step, starting with recording raw data, that are inherently non-uniformly sampled. Subsequently, the raw staggered SAR data are resampling to a uniformly spaced grid and then the compression is applied in range and azimuth.

It is important to select a Sequence of PRIs that will be repeated periodically. The PRI sequence is characterized by an interval between the maximum and the minimum PRIs bound. The maximum PRI should be small enough to ensure that in azimuth signal two successive samples are never missed. While PRI minimum limit should be kept large enough to contain range ambiguities. It is usually is possible to adopt two kind of strategy according to applications, fast and slow change PRI. In this thesis it will be adopted fast change PRI, i.e. sequence with increasing PRI. Fast PRI change limits maximum pulse separation and permits recovering missing samples by interpolation [9].

In addition the mean PRI is decreased, i.e. if the signal averagely oversampled in azimuth, it is possible to prevent high sidelobe in azimuth impulse response and accurately interpolate the data on a uniform grid.

3.2 Interpolation Method

The interpolation method allows recovering uniformly sampled data from staggered SAR raw data, which are inherently non-uniformly sampled.

During the signal reconstruction of Staggered SAR, the range offset is neglected. In staggered SAR case, all samples received from the same range have the same range curvature. The time difference between the samples in the non uniform and uniform grids is the order of tenths of a millisecond and for this small value it can be neglected.

3.2.1 BLU (Best Linear Unbiased) Interpolation

The Blue is based on the linear estimator which is unbiased and has minimum variance. BLUE interpolation allows to overcome some estimation problems, like MVUE that cannot be found or indeed the PDF (Probability Density Function) of the data is itself unknown (only the second-

order statistics are known in the sense that they can be estimated from data). In such cases, one solution is to assume a functional model of the estimator, as being linear in the data, as the best linear unbiased estimator (BLU).

Let us consider $u(t)$ be the raw azimuth signal, with a zero-mean complex random process. The power spectral density (PSD) of $u(t)$ is proportional to antenna power pattern:

$$P_u(f)=U(f)*U^*(f)=\sin^4(\pi\frac{L}{2v_S}f)/(\pi\frac{L}{2v_S}f)^4 \tag{23}$$

where $U(f)$ is the spectrum of $u(t)$.

In the presence of Additive White Gaussian Noise the autocorrelation function $R_{un}(\xi)$ of the complex random process $u(t)$ is given by [4]:

$$R_{un}(\xi)=\frac{1}{SNR}\delta(\xi)+\frac{SNR-1}{SNR}R_u(\xi) \tag{24}$$

where δ() is the Kronecker delta. $R_u(\xi)$ is normalized autocorrelation function without white noise.

$$R_u(\xi)=0, |\xi|\geq\frac{L}{v_s} \tag{25}$$

the estimator is given by:

$$\hat{u}(t_{\text{int}})=\underline{u}^T\underline{\underline{G}}^{-1}\underline{r} \tag{26}$$

where $\underline{u}$ is a column vector collecting the samples $u(t_q), q=1..Q$ and $\underline{r}$ is a column vector, whose the element is given by

$$r_q=R_{un}(t_{\text{int}}-t_q), \qquad q=1..Q \tag{27}$$

the matrix $\underline{\underline{G}}$ has the element given by [4]:

$$g_{bs}=R_{un}(t_q-t_s), \qquad q=1..Q, \quad s=1..Q \tag{28}$$

the variance relative to estimator is:

$$E\{|\hat{u}(t_{\text{int}})|-u(t_{\text{int}})\}/E\{|u(t_{\text{int}})|^2\}=1-\underline{r}^T\underline{\underline{G}}^{-1}\underline{r} \tag{29}$$

3.4 On-board Processing

The SAR raw data are stored on the satellite, transmitted to the ground station and transferred to the processing facility. This process becomes complicate to do with global coverage and very high resolution SAR systems because it is related to a huge amount of data. This makes necessary to use various signal processing and compression techniques to reduce the amount of data. The current goal is to overcome the limitations in terms of memory bandwidth and On-board computation. In addition, to meet the requirements of azimuthal ambiguity, a pulse repetition frequency (PRF) much higher than the required processed Doppler bandwidth (PBW) is often desirable. For this reason arise the necessary of on board processing.

On-board data processing consisting of the data acquisition, transfer, storage, data compression or reduction, transmission to the ground station, ground processing, and archiving.

The advantages of on-board processing [11] -[12]:

- reduction of the amount of raw data to be stored in the satellite memory
- a small number of ground stations is required
- digital filter that integrates raw data compression provides adequate signal sampling
- fewer data transmitted to the ground

The steps that permit to reduce the data volume before the downlink are the following: resampling, Doppler filtering and decimation, followed after by resampled and decimation. After the downlink follow: filter compensation, SAR processing, Focused SAR data. This step are shown in Fig. 10.

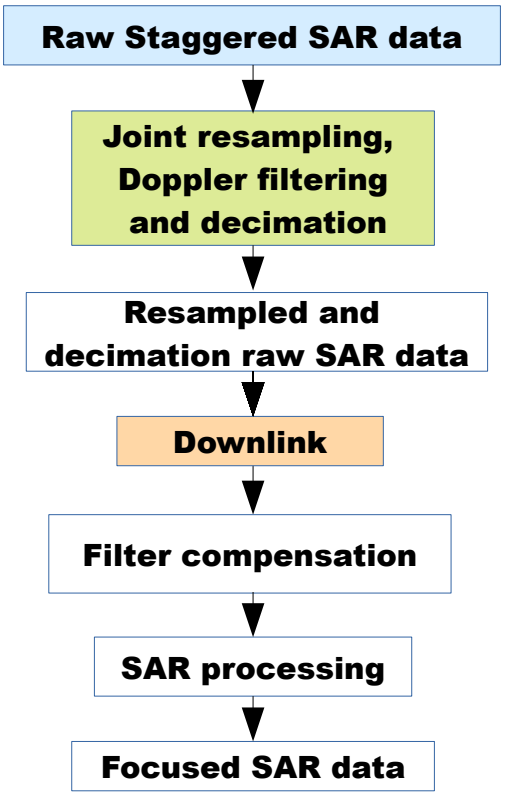

Fig. 10 Block Diagram of data volume reduction strategy

The resampling allows to pass a uniform grid reducing the "blind ranges". Doppler filtering reduces additional ambiguous energy, if it is performed before the decimation. The Doppler filter is conducted in time domain using a finite impulse response (FIR) filter with a relatively small number of taps. The decimation is associated with straightforward implementation and a much lower computational cost.

3.4.1 Finite Impulse Response (FIR) Filter Design

The Finite Impulse Response (FIR) filter reduce sidelobes, interference, and noise in Fourier transform data. In this thesis it will be considered Wiener filter that is a particular case of FIR filter.

The Wiener filter is a digital filter used for signal processing on a statistical basis characterized by linear time-invariant (LTI) filtering. The goal of a filter is to remove noise from the signal. The filters are designed for specific frequency response and can separate the signal from the noise as long as they occupy different frequency bands. The Filter Wiener overcomes this limitation by addressing the problem of filtering with a statistical approach.

The input signal $w[n]$ with order N and with coefficients $a_i, i=0,\ldots,N$, is convolved with the Wiener filter $g[n]$. The output $x[n]$ is compared to a reference signal $s[n]$ to obtain the filtering error $e[n]$ (fig.11):

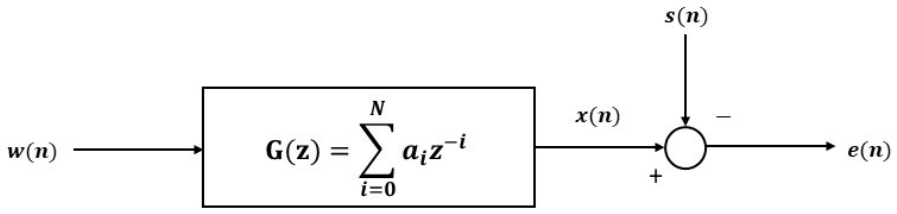

Fig.11 Block diagram view of the FIR Wiener filter

the output is given by the expression:

$$x[n]=\sum_{i=0}^{N} a_i w[n-i] \tag{30}$$

The residual error is $e[n]=x[n]-s[n]$ and the goal of Wiener filter is to minimize the mean square error as follow:

$$a_i=arg\{min\, E[e^2[n]]\} \tag{31}$$

where $E[.]$ is expectation operator.

The mean square error (MSE) may be rewritten as [13]:

$$\begin{gathered} E\{e^2[n]\}=E\{(x[n]-s[n])^2\}= \\ E\{x^2[n]\}+E\{s^2[n]\}-2E\{x[n]s[n]\}= \\ E\{(\sum_{i=0}^{N} a_i w[n-i])^2\}+E\{w^2[n]\}-2E\{\sum_{i=0}^{N} a_i w[n-i]s[n]\} \end{gathered} \tag{32}$$

deriving this expression with respect to the coefficients a_i, it is possible to find the expression that minimizes the vector $[a_0,\ldots,a_N]$:

$$\begin{gathered} \frac{\partial}{\partial a_i} E\{e^2[n]\}=2E\{(\sum_{j=0}^{N} a_j w[n-j])-2E\{s[n]w[n-i]\}= \\ 2\sum_{j=0}^{N} E\{w[n-j]w[n-i]\}-2E\{w[n-i]s[n]\} \end{gathered} \tag{33}$$

with $i=0,\ldots,N$.

If the sequence s[n] and w[n] are stationary is possible define:

$$R_w[m]=E\{w[n]\,w[n+m]\} \quad \text{and} \qquad R_{ws}[m]=E\{w[n]s[n+m]\} \tag{34}$$

where R_w is the autocorrelation of $w[n]$ and R_{ws} is the cross-correlation between $w[n]$ and $s[n]$

The derivative of the MSE may be rewritten as [15]-[16]:

$$\frac{\partial}{\partial a_i}E\{e^2[n]\}=2\sum_{j=0}^{N}R_w[j-i]a_j-2R_{sw}[i] \tag{35}$$

Imposing the derivative be equal to zero results is achieved

$$\sum_{j=0}^{N}R_w[j-i]a_j=R_{sw}[i] \tag{36}$$

in matrix form [17]

$$\begin{bmatrix} R_w[0] & R_w[1] & \cdots & R_w[N] \\ R_w[1] & R_w[0] & \cdots & R_w[N-1] \\ \vdots & \vdots & \ddots & \vdots \\ R_w[N] & R_w[N-1] & \cdots & R_w[0] \end{bmatrix}\begin{bmatrix} a_0 \\ a_1 \\ \vdots \\ a_N \end{bmatrix}=\begin{bmatrix} R_{sw}[0] \\ R_{sw}[1] \\ \vdots \\ R_{sw}[N] \end{bmatrix} \tag{37}$$

These matrices are not singular, so there is only one solution in determining the coefficients of the Wiener filter.

3.4.2 Data Volume Reduction in Staggered SAR

Staggered SAR system, which is characterized by a variable PRI, needs a high value of mean pulse repetition frequency (PRF) for oversample in azimuth. The higher mean PRF leads to increased range ambiguities and an increased data volume. On the other hand, limited resources on board satellite (transmitted power) and the dimension of the antenna on the ground, reduce the downlink data volume, which can be received by a ground station. It is necessary a strategy that reduces data volume before the download, indeed, in case the mean PRF is much higher than the processed Doppler bandwidth, it can be reduced by on-board Doppler filtering and decimation [4]. In Fig. 12 shows the step that reduces the data volume: resampling, filtering and decimation.

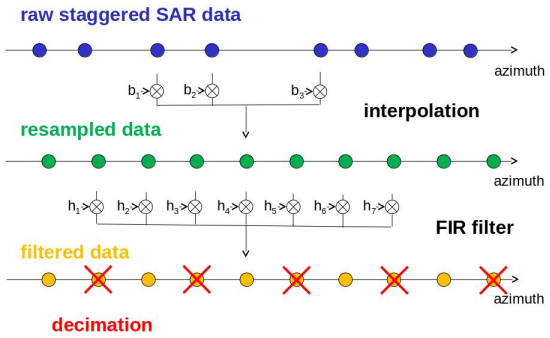

Fig. 12 Processing data for Staggered SAR. Interpolation, Doppler filtering and decimation [4].

The resampling permits to modify the sampling frequency and permits to pass from a non-uniformly raw data to the uniform grid, with the advance of remove gaps that are present in raw staggered SAR data. The better way to permit this, is applying BLU interpolation.

The Doppler filtering removes part of ambiguous energy. The filter introduces a distortion of the Doppler spectrum of the signal, which can be compensated on the ground in the SAR processing[4].

The decimation reduces the sampling frequency. If resampling, Doppler filtering and decimation can also jointly performed Fig. 13.

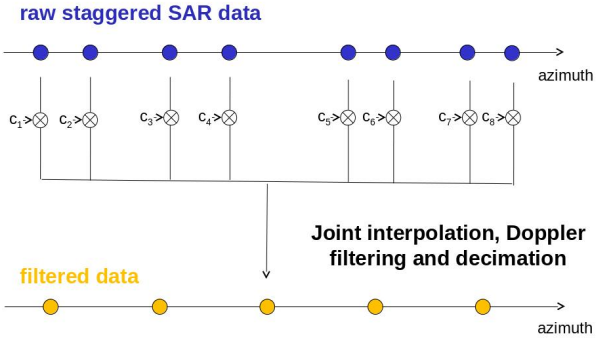

Fig. 13 Interpolation, Doppler filtering and decimation jointly performed [4].

If data were decimated before the downlink, would occur high degradation of Azimuth-Ambiguity to Signal Ratio (AASR). In addition, if Doppler low-pass filtering is performed before decimation, the additional ambiguous energy due to decimation can be reduced.

Applying Doppler filtering is possibly performed in the time domain using finite impulse response (FIR) filter on data. Moreover, for a Staggered SAR system, a rational decimation factor can be selected without a significant increase in the computational cost, just by properly choosing the resampling frequency. [14]

The output grid data is then obtained by a decimation of the filtered data by the factor of 2 or 3. The decimation reduces the sampling rate.

4 Data Volume Reduction in Staggered SAR with a Limited Number of Taps

The previous strategy permits to reduce the downlink data, does not take into account the limited memory of the FPGA on board satellite. In this section it is proposed a sub optimal method that takes into account the limited memory on board satellite and is discussed the step that permits to reduce the data volume onboard SAR.

In the years the evolution and complexity of SARs have led to a greater increase in data volume. The Staggered SAR system, which is characterized by a variable PRI, needs a high value of mean pulse repetition frequency (PRF) for oversample in azimuth. The higher mean PRF leads to increased range ambiguities and an increased data volume. The memory on board satellite is limited and for this reason, during onboard processing, it is necessary to select a limited number of azimuth samples (taps). For these reasons, it is necessary to find a system that allows reducing the data volume. The idea is to transform the raw staggered SAR data to a minor sampling PRF output virtual grid. Proceed by selecting a certain number of taps from raw data, including missing samples (white points), to evaluate a single output sample, as shown in Fig. 14.

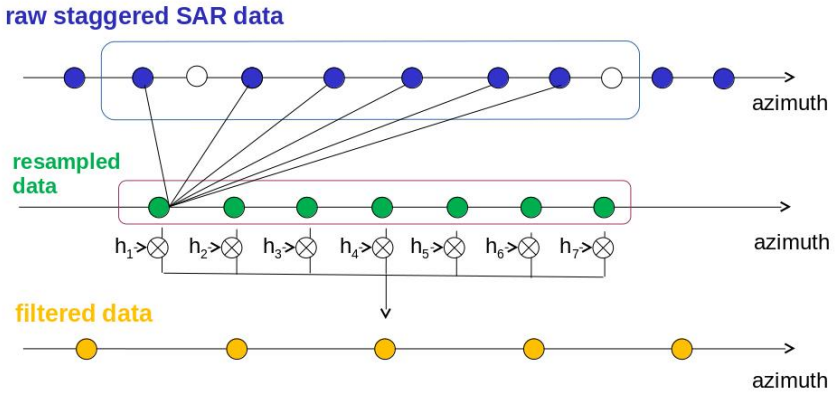

Fig. 14 Processing data for Staggered SAR with limited numbers of taps.

The blue points along the azimuth line are taps of raw staggered SAR data and it is selected only some taps of them.

The raw data selected are non uniformly sampled and are characterized by gaps, white points in Fig. 14. From desire PRF mean in transmitting is possible to obtain a sequence of PRI.

The resampling permits recovering uniformly sampled data from raw data. The resampled taps, green points Fig. 14, are also selected around the output point and the numbers of resampled taps depend on the input taps. The resampled data are obtained applying BLU interpolation (section 3.2.1) to the raw data. In particular each resampled tap (in green) is obtained from BLU interpolation of all selected taps (in blue) of the raw data except missing samples (in white) (Fig. 14). The resampled data are uniformly distributed and without gaps. This procedure is repeated for each tap of resampled data.

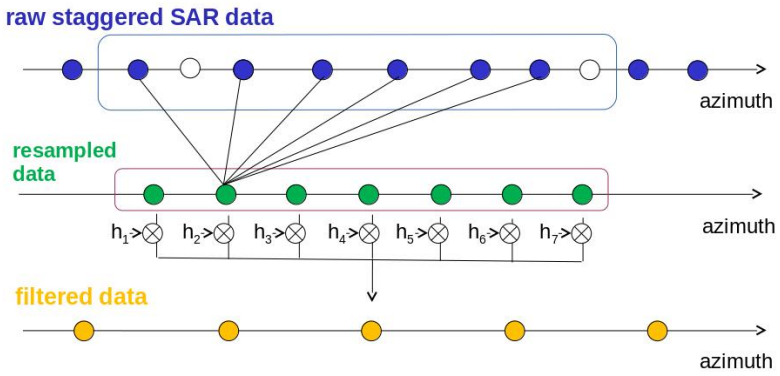

Fig. 15 Processing data for Staggered SAR with limited numbers of taps.

Once the sequence of resampled data is obtained, is possible to apply the Doppler filtering to resampled data. The Doppler filtering is performed in the time domain over the resampled grid using a finite impulse response (FIR) filter with a small number of taps[14].

The output is obtained from a linear combination of resampled taps, yellow points (Fig. 15). Each output point is obtained shifted the taps along the azimuth line. For each output corresponds a new section of the raw data grid and new resampled data grid. The procedure is repeated every time selecting a new sequence of raw data.

The length of each section of the raw data grid is constant for each output and it is called N_{taps}. The length of each resampled data grid is constant for each output and is called $N_{\text{taps filter}}$.

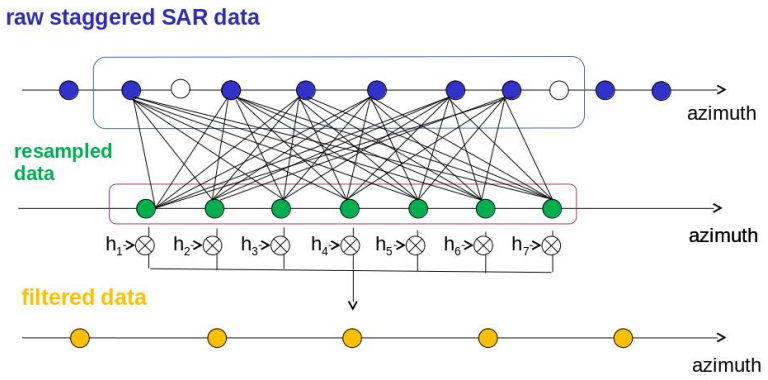

Fig. 16 Processing data for Staggered SAR with limited numbers of taps.

The PRF in output will be given by the multiplication of the PBW (Processed Doppler Bandwidth) by a margin factor.

$$PRF_{out} = bw_{margin} * PBW \tag{38}$$

For example $bw_{margin} = 1.2$ corresponds to 20% of bandwidth margin.

Summarizing the passages:

- Select the N_{taps} from the staggered grid closest to the output tap
- Create a new resampled grid with $N_{\text{taps filter}}$ around the output tap with the same length of staggered taps.
- Apply BLU interpolation from staggered grid section to the resampled taps.
- Apply FIR filter for each output sample over the resampled grid yielding the output tap value.

5. Results

5.1 Performance Analysis

During the performance analysis, different parameters were examined and the performance evaluated for different cases.

5.2 Input Parameters

In order to analyze and compare different performances, an illustrative scenario is considered, in particular Tandem-L mission proposal. The goal is to image from an orbit height of 740 km a swath of 350 km with 7.0 m azimuth resolution in L-band, using a parabolic reflector antenna architecture [18].

The performance of a system based on staggered SAR depends on several system and processing parameters.

For a conventional SAR system the parameters in the input are different:

- orbit height
- the wavelength
- the antenna characteristics
- the transmitted chirp bandwidth,
- the processing window and etc.

For a staggered SAR is necessary to consider also other parameters like:

- resampling method,
- the processing strategy,
- mean PRF,
- the number of subcycles for the sequence of PRI etc.

If the data processing is done on board satellite it is to necessary consider also the number of taps, bandwidth margin and type of filter.

Tab. 2 Set of system and processing parameters of a Staggered SAR system.

Parameter	**Value**
Radar wavelength	0.2384 m (L-band)
Orbit height	740465 m
Minimum incidence angle	26.3°
Maximum incidence angle	46.975°
Mean Duty cycle	4%
Chirp bandwidth	84 MHz
Range sampling frequency	92.4 MHz
Number of concatenated sequences	7
Tilt angle	32.155°
Antenna diameter	15 m
Mean PRF to TX	2700 Hz
Processed Doppler bandwidth	1128 Hz
Resampling method	BLU interpolation
Azimuth processing window	Hamming window with $\alpha = 0.6$
Range processing window	Hamming window with $\alpha = 0.6$
Numbers of taps	various values
Bandwidth margin	From 10% to 30%
Filter type	Wiener filter

5.3 Simulation Tool

The algorithm that allows reducing the data volume considering a limited number of taps was implemented with IDL (Interactive Data Language). The IDL is a scientific programming language used for data analysis, for interactive processing of large amounts of data and image processing. The simulator starts from point target with on a specific slant range and generates raw staggered data taking into account antenna pattern and azimuth modulation.

Two tools will be considered, one for staggered SAR called “Main Staggered” described in section 3.4.2 and the other one for staggered SAR On-board processing called “Main Staggered Obp” described in section 4. In each tool, different strategies are used to interpolate the staggered raw data in uniform sample raw data. Then in both tools the uniform sample raw data is passed to conventional SAR processor, that yields the impulse response, from which the AASR, AASR Degradation, Azimuth Resolution, Pulse to Sidelobe Ratio (PSLR) parameters are computed.

In both tools there are input parameters with the different values but only in the “Main Staggered Obp” are present: bandwidth margin, rough output PRF and numbers of taps. The simulator is run once for different range points uniform spaced between the near and far range.

In the end of this tools are generate AASR, AASR Degradation, Azimuth Resolution, PSLR, Impulse Response and Transfer Function for different values are generated. All these parameters are analyzed for both tools and make the comparison each other.

5.4 Output Parameters

Taking into account the input parameters and set of system it is possible to evaluate the performance of a staggered SAR system. In particular in this work has been estimated some parameters for a Staggered SAR, considered as reference, and Staggered SAR, after on board processing, with limited numbers of taps.

- AASR (Azimuth Ambiguity to Signal Ratio) is a measure of the azimuth ambiguity of SAR images. The AASR parameter is the ratio of the power of the azimuth ambiguities to the power of the signal. The azimuth ambiguities take into account the aliased part of the Doppler spectrum and the power of the signal is the part of Doppler spectrum within the processed bandwidth

$$AASR = \frac{\sum_{\substack{m=-\infty \\ m\neq 0}}^{\infty} \int_{f=-B_p/2}^{B_p/2} G^2(f+mPRF)Q^2(f)\,df}{\int_{f=-B_p/2}^{B_p/2} G^2(f)Q^2(f)\,df} \qquad (39)$$

  where $G^2(f)$ is two-way antenna power pattern as a function of the Doppler frequency, B_p is the processed Doppler bandwidth, $Q(f)$ accounts for the amplitude weighting of the Doppler spectrum in the processing.

  The very low AASR levels indicate that an even higher azimuth bandwidth could be processed, leading to a better resolution.

- The ISLR (Integrated Side-Lobe Ratio) parameter is the ratio of the energy of all sidelobes to the main lobe energy. It characterizes the ability to detect weak targets in the neighborhood of bright targets.

  The ISLR strongly depends on the azimuth amplitude weighting, applied in the processing.

$$ISLR = \frac{Signal\ \ Energy\ \text{in}\ \ Mainlobe}{Integrated\ \ Signal\ \ Energy\ \text{in}\ \ Sidelobes} \qquad (40)$$

- For a better comparison is possible to take into account AASR degradation that is the difference between reference AASR and AASR after on board processing. Can also be

considered as the difference between ISLR after on board processing and ISLR reference [19].

$$AASR_{degradation} = ISLR_{obp} - ISLR_{reference} \tag{41}$$

- PSLR is defined by the ratio of the largest level of sidelobes compared to the peak level of mainlobe. It represents the ability of the SAR to identify a weak target from a nearby strong one.

$$PSLR = 10\log_{10}\frac{I_s}{I_m} \tag{42}$$

Where I_s stands for the peak intensity of the most intensity sidelobe and I_m stands for the peak intensity of the mainlobe.

- It is also possible to evaluate the performance of antenna considering radiation pattern, i.e. the amplitude of mainlobe and sidelobe for ideal staggered SAR and for a limited number of taps as shows in Fig. 17-18.

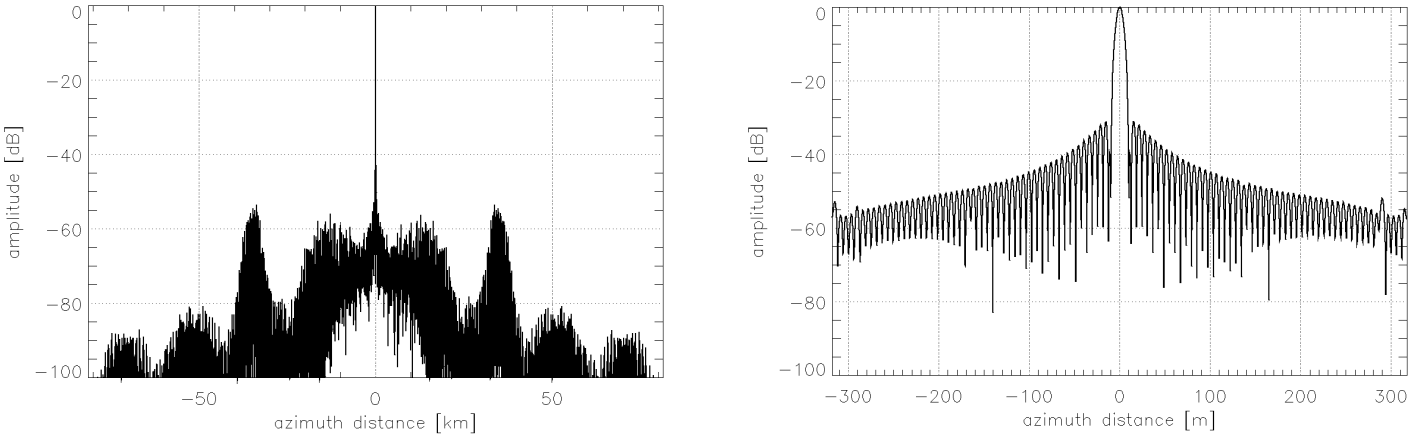

Fig. 17 One-dimension simulation for a Staggered SAR system. The amplitude of the focused azimuth signal in dB for near range 324 km. The image on the right shows the zoom of the mainlobe.

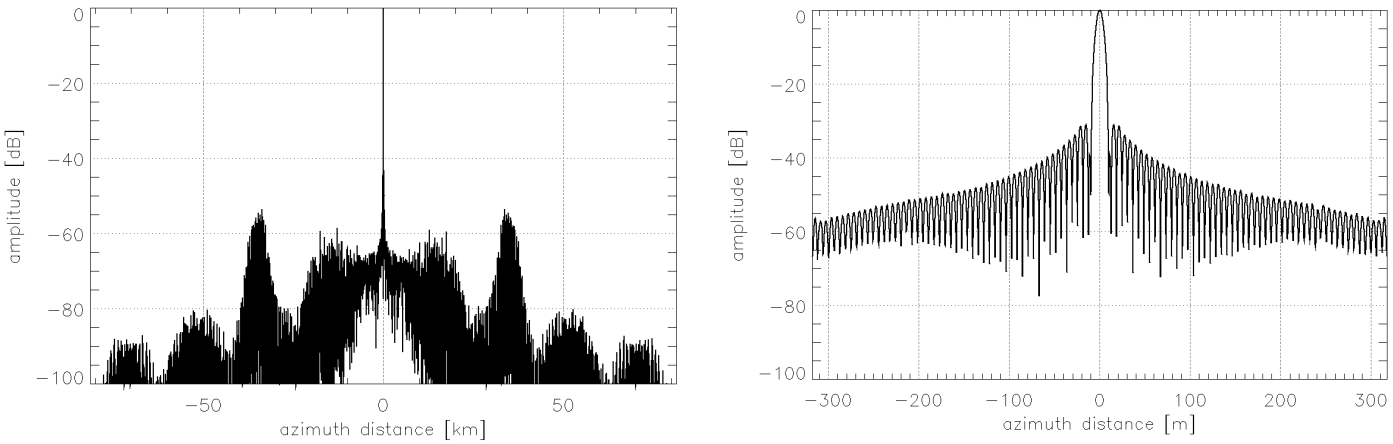

Fig. 18 Simulation on board processing with 15 taps. The amplitude of the focused azimuth signal in dB for near range 324 km. The image on the right shows the zoom of the mainlobe.

5.5 Impact on Performance of the Features Peculiar of a Staggered SAR System

In the following the impact of performance for high-resolution wide-swath SAR system, are considered. The performance of the algorithm described in 3.4.2 and the suboptimal algorithm described in section 4 will be analyzed. Let's consider for the simulation the characteristics described in Tab.2 selecting different numbers of taps and bandwidth margin for single and quad polarization.

5.5.1 Impact of Performance in Single and Quad Polarization for Different Numbers of Taps and Bandwidth Margin

In this work several parameters will be analyzed (AASR, AASR degradation, PSLR and azimuth resolution) for the Single-pol and Quad-pol mode. First of all let’s consider Simulation for Single-Pol for PRF=2700 Hz, margin bw= 20% and numbers of taps = 5,9,13,17 as shown in Fig.19 and Fig.20.

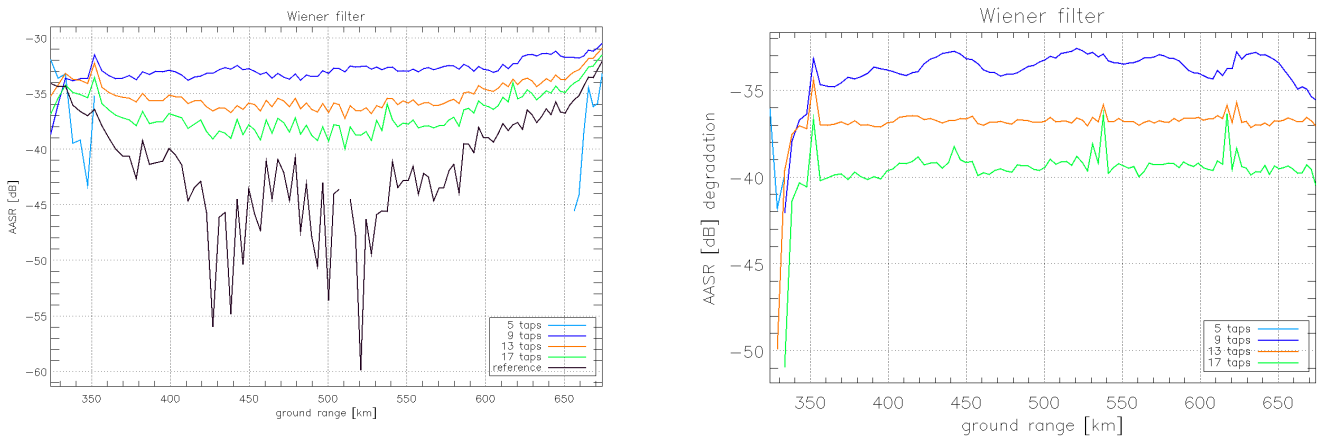

Fig. 19: AASR (right) (a) and AASR degradation (left) (b) versus ground range, after applied Wiener filter for different numbers of taps and single-polarization with bw margin=20%.

The black curve in fig.19a has a concave shape over the swath with lower levels in middle range and with local performance oscillations. The smooth concave trend can be related to defocusing of the reflector patterns, an effect of the offset with respect to the focal plane [20]. In near and far range the elements are positioned at extremes of the feed therefore further away from paraboloid's focus. On the other side in the center of swath, the elements are closer to the focus and there is a better resolution. By applying the suboptimal algorithm the concave shape is reduced by decreasing the number of taps. In fact, for 9 taps there is no longer concave shape.
The trend of the best AASR occurs for 17 taps, is closer to the reference trend and has low degradation (fig. 19b). As shown in fig 19a-19b, the tool cannot evaluate the performance for 5 taps.

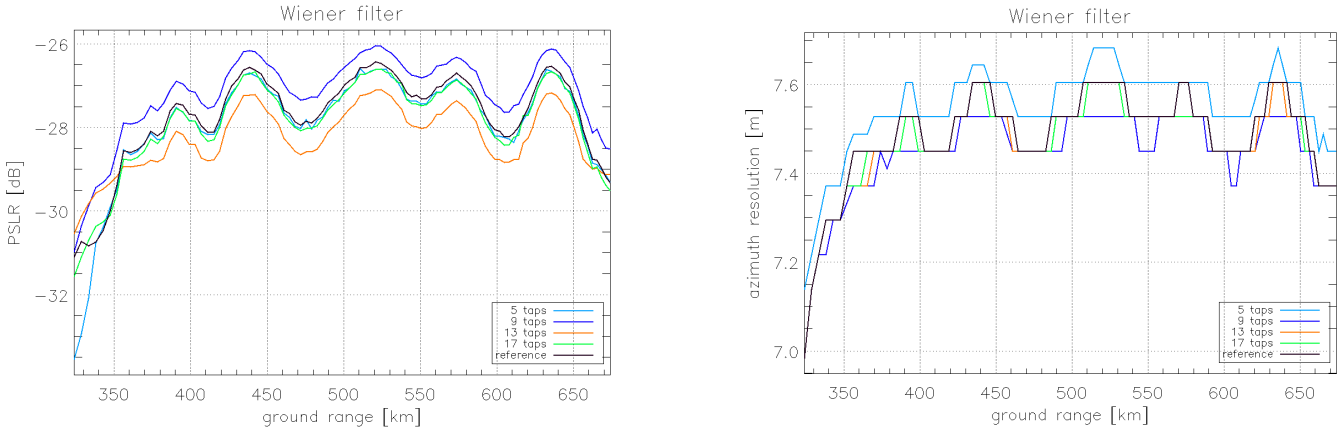

Fig. 20: PSLR vs ground range (right) (a) and azimuth resolution vs ground range (left) (b), after applied Wiener filter for different number of taps and single-pol with bw margin=20%.

The shape PSLR curves (fig.20a) depend on the ratio between the intensity of sidelobes and main lobes as defined 5.4 section.
The azimuth resolution fig. 20b is taken in account for possible distortions introduced by resampling and possible degradation considering the suboptimal algorithm. This parameter is estimated directly from the focused impulse response in time domain after interpolation.

Tab.3: Worst value for different parameters and taps for the case of single-pol with bw margin=20%.

Number of taps	**Worst values of AASR [dB]**	**Worst values of AASR degradation [dB]**	**Worst values of azimuth resolution [m]**	**Worst values of PSLR [dB]**
5	-31.951484	-36.067617	7.6820114	-26.583749
9	-30.472493	-32.596711	7.5268192	-26.043206
13	-30.889981	-34.415457	7.6044153	-27.086627
17	-31.500685	-36.378350	7.6044153	-26.593930
Reference	-32.092174		7.6044153	-26.427804

Let's consider now the simulation for Quad-Pol for PRF=2*2000 Hz, margin bw= 20%, numbers of taps = 5,9,13,17 and HH-VH & VV-HV polarization.

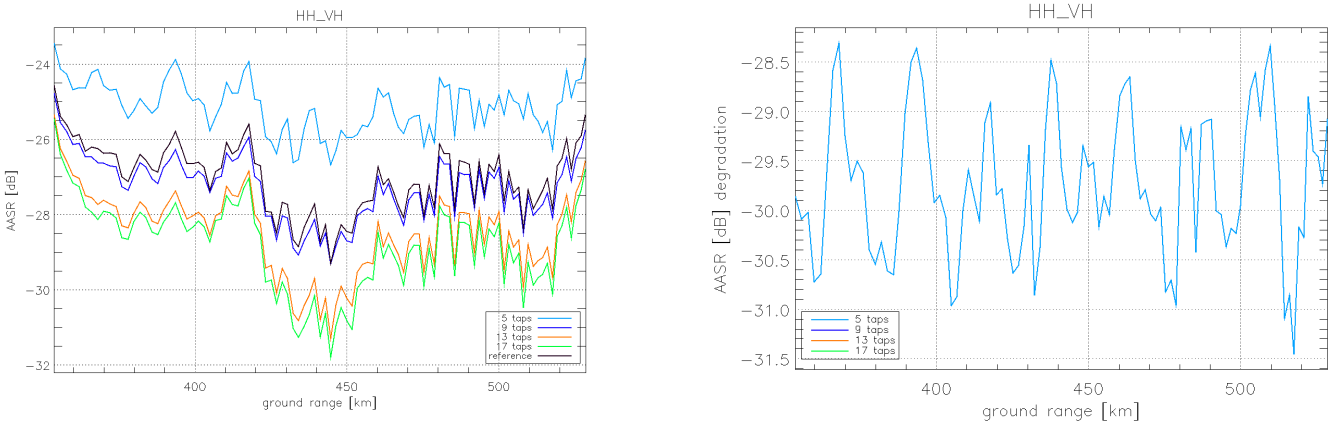

Fig. 21: AASR vs ground range (right) (a) and AASR degradation vs ground range (left) (b), for HH-VH polarization, for different number of taps and quad-pol with bandwidth margin=20%.

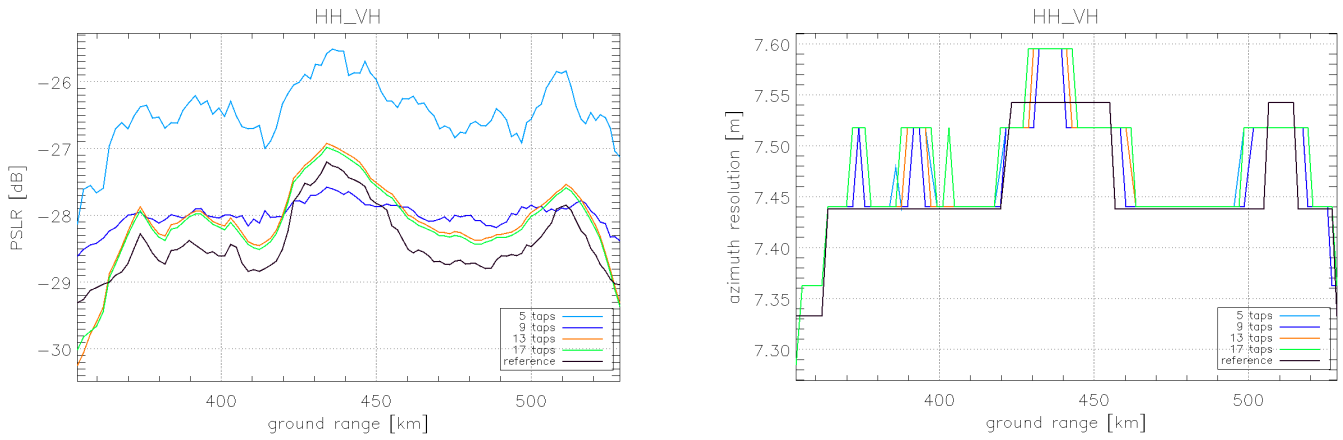

Fig. 22: PSLR vs ground range (right) (a) and Azimuth Resolution vs ground range (left) (b), for HH-VH polarization, for different numbers of taps and quad-pol with bw margin=20%.

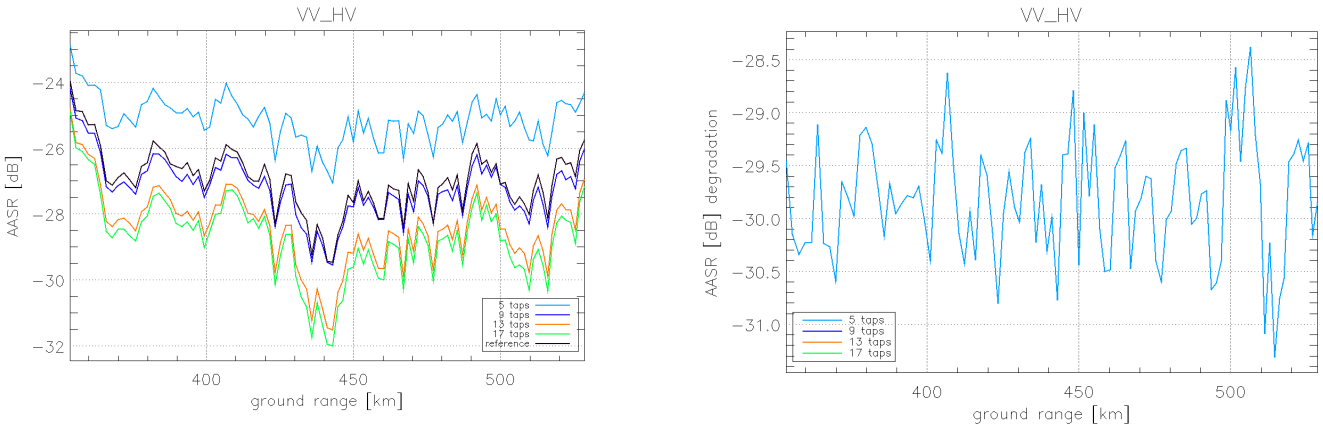

Fig. 23: AASR vs ground range (right) (a) and AASR degradation vs ground range (left) (b) for VV-HV polarization, for different numbers of taps and quad-polarization with bandwidth margin=20%.

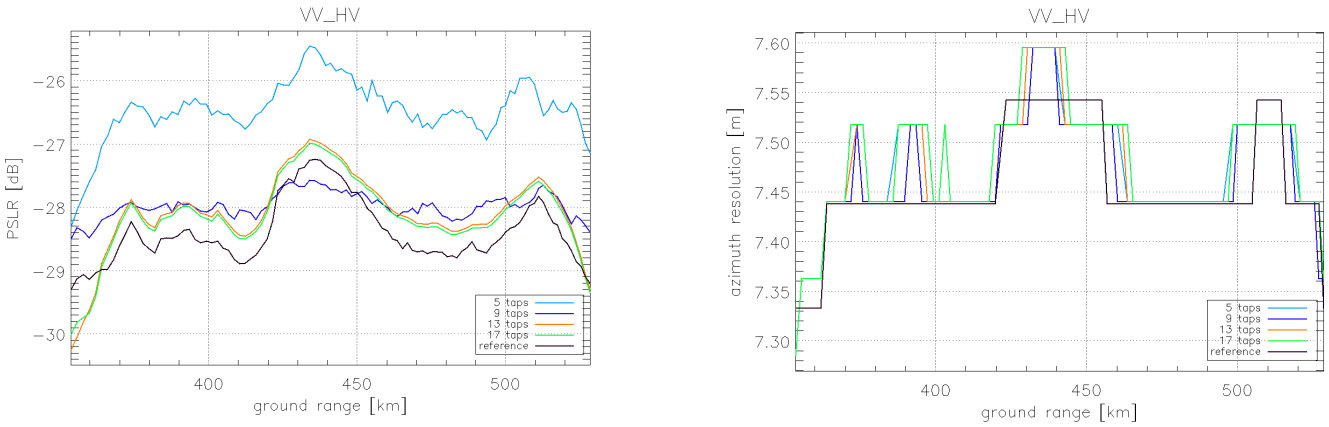

Fig. 24: PSLR vs ground range (right) (a) and azimuth resolution vs ground range (left) (b) for VV-VH polarization, for different numbers of taps and quad-pol with bandwidth margin=20%.

A joint processing of the data acquired by quad-pol mode could lead significant improvement of the AASR.

In quad polarization, the distortions of azimuth resolution for 5 taps are reduced.

In the fig. 22a, 24a the PSLR curve are similar and the same for azimuth resolution fig. 22b and 24b. The graphics change in the near range for AASR an AASR degradation fig.21 and fig.23, that depends for different direction of polarization.

Comparing the Figs 19b, 21b, 23b it is possible to observe that for quad-pol mode there is not degradation for 9, 13, 17 taps.

Tab.4: Worst value for different parameters and taps for the case of HH-VH with bandwidth margin=20%.

Number of taps	**worst values AASR HH_VH**	**worst values AASR degradation HH_VH**	**worst values azimuth resolution HH_VH**	**worst values PSLR HH_VH**
5	-23.452905	-28.312819	7.5949512	-25.512607
9	-24.779403	*	7.5949512	-27.579749
13	-25.352075	*	7.5949512	-26.920881
17	-25.454325	*	7.5949512	-26.982937
Reference	-24.580017		7.5423369	-27.202831

In the case of quad-pol there is a remarkable improvement in ambiguity-to-signal ratios, and improvement in azimuth resolution, while the value of PSLR is variable with the number of taps as shown in tab. 3 and tab. 4-5, this improvement it is also related to a higher PRF used for quad-pol.

The symbol *, that is present in different Tabs, means that the tool cannot evaluate accurately the degradation.

Tab.5: Worst value for different parameters and taps for the case of VV-HV with bandwidth margin=20%.

Number of taps	**Worst values AASR VV_HV**	**Worst values AASR degradation VV_HV**	**Worst values azimuth resolution VV_HV**	**Worst values PSLR VV_HV**
5	-22.888458	-28.382167	7.5949512	-25.456834
9	-24.203410	*	7.5949512	-27.574724
13	-24.806676	*	7.5949512	-26.930915
17	-24.899067	*	7.5949512	-26.983858
Reference	-23.970188		7.5423369	-27.238457

Let's consider a different value of bandwidth margin 30%. In the case of single- pol for PRF= 2700 Hz and numbers of taps= 5, 9, 13, 17 it is possible obtain the following graphics:

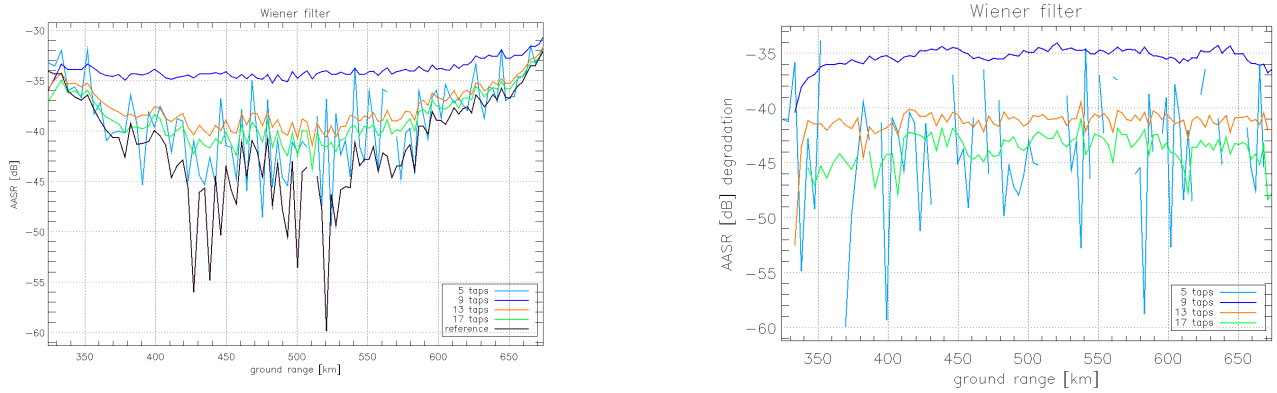

Fig. 25: AASR vs ground range (right) (a) and AASR degradation vs ground range (left)(b), after applied Wiener filter for different numbers of taps and single-polarization with bandwidth margin=30%.

In fig. 25b the tool cannot evaluate accurately the degradation for 5 taps.

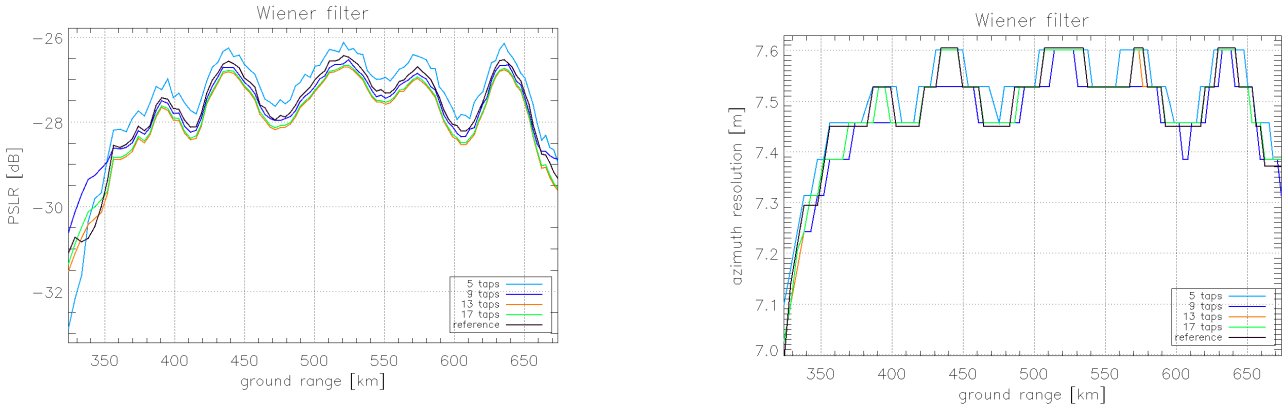

Fig. 26: PSLR vs ground range (right)(a) and azimuth resolution vs ground range (left)(b) versus ground range, after applied Wiener filter for different numbers of taps with bw margin=30%.

Making the comparison of fig. 20b and 26b it is possible notice that the azimuth resolution for 5 taps is better for bandwidth margin 30%.

Applying 30% of bandwidth margin it is possible to observe AASR and PSLR for 5 taps (Figs. 25A, 26a), which was not possible by a margin of 20% (Figs. 19a, 20a).

Tab.6: Worst value for different parameters and taps for the case of single-pol with bw margin=30%.

Number of taps	**Worst values of AASR [dB]**	**Worst values of AASR degradation [dB]**	**Worst values of azimuth resolution [m]**	**Worst values of PSLR [dB]**
5	-31.618604	-33.868438	7.6000699	-26.122164
9	-30.718090	-34.014614	7.6000699	-26.526093
13	-31.644299	-39.363323	7.6000699	-26.703542
17	-31.949110	-40.898365	7.6000699	-26.665161
Reference	-32.092174		7.6044153	-26.427804

Comparing the value for single-pol for bw= 20% (tab. 3) and 30% (tab. 6) it is possible to observe that AASR and AASR degradation for 5 taps with margin 30% is worst but for 9, 13, 17 it is worst for margin of 20%. While PSLR is worst for margin of 30% for taps 5,13,17 and for 9 taps is worst for a margin of 20%.

Let's consider the last simulation for Quad-Pol for PRF=2*2000 Hz, margin bw= 30% and numbers of taps = 5, 9, 13, 17 and HH_VH & VV_HV polarization.

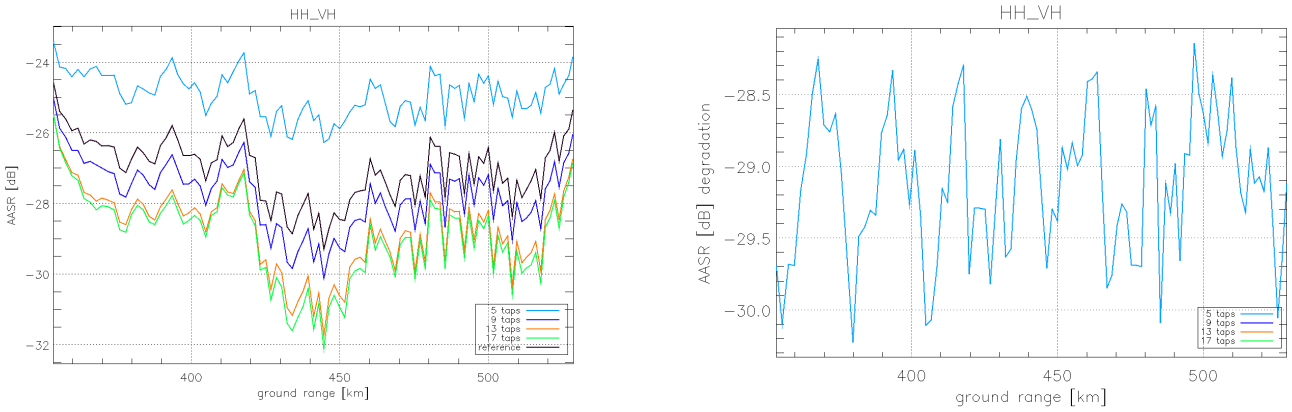

Fig. 27: AASR vs ground range (right) (a) and AASR degradation vs ground range (left) (b), for HH-VH polarization, for different numbers of taps and quad-polarization.

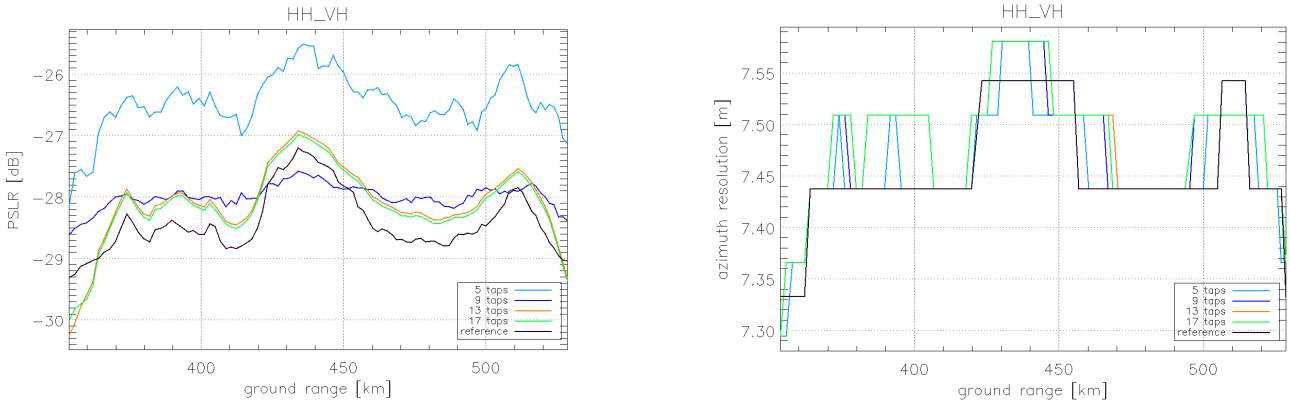

Fig. 28: PSLR vs ground range (right) (a) and azimuth resolution vs ground range (left) (b) for HH-VH polarization, for different numbers of taps and quad-polarization.

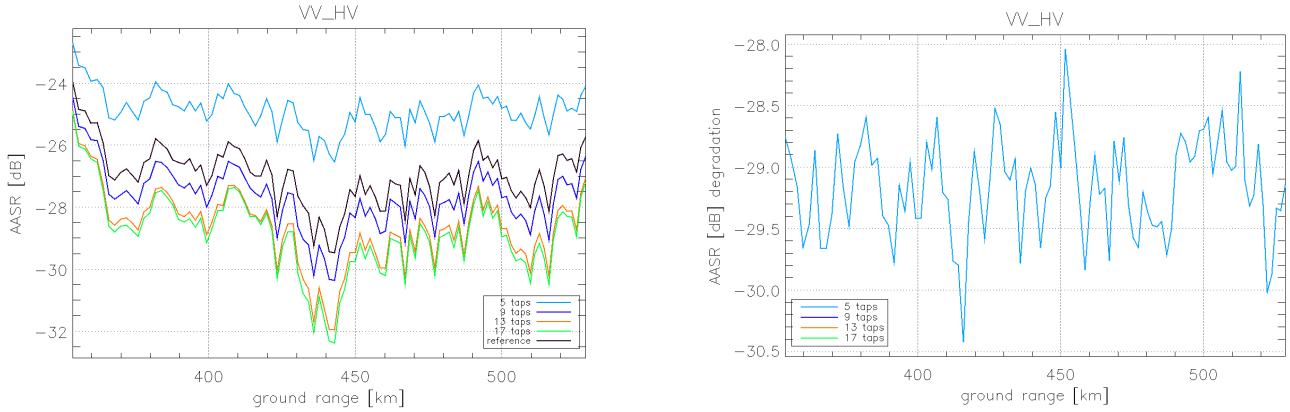

Fig. 29: AASR vs ground range (right) (a) and AASR degradation vs ground range (left) (b), for VV-HV polarization, for different numbers of taps and Quad-pol.

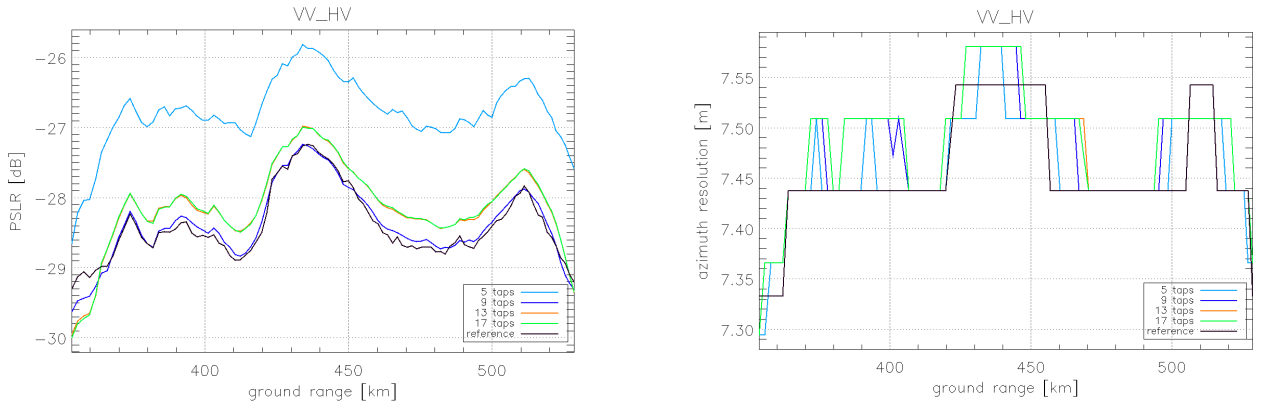

Fig. 30: PSLR vs ground range (right) (a) and azimuth resolution vs ground range (left) (b) for VV-HV polarization, for different numbers of taps and quad-polarization.

Tab.7: Worst value for different parameters and taps for the case of HH-VH with bw margin=30%.

Number of taps	**worst values AASR HH_VH**	**worst values AASR degradation HH_VH**	**worst values azimuth resolution HH_VH**	**worst values PSLR HH_VH**
5	-23.414145	-28.144717	7.5803897	-25.880638
9	-25.032324	*	7.5803897	-27.226286
13	-25.474667	*	7.5803897	-26.996938
17	-25.498763	*	7.5803897	-26.996112
Reference	-24.580017		7.5423369	-27.202831

Tab.8: Worst value for different parameters and taps for the case of VV-HV with bw margin=30%.

Number of taps	**worst values AASR VV_HV**	**worst values AASR degradation VV_HV**	**worst values azimuth resolution VV_HV**	**worst values PSLR VV_HV**
5	-22.726066	-28.044706	7.5803897	-25.813625
9	-24.469015	*	7.5803897	-27.240732
13	-24.901285	*	7.5803897	-26.977245
17	-24.942359	*	7.5803897	-26.989367
Reference	-23.970188		7.5423369	-27.238457

Comparing the value for quad-pol for bw= 20% (tab. 4-5) and 30% (tab. 7-tab. 8) it is possible to observe that AASR and AASR degradation for 5 taps is worst for a margin of 30%, while for 9,13,17 values it is worst for 20%. Resolution in azimuth slightly improves for 30% of bandwidth margin. The value of PSLR is worst for 5,13,17 for margin of 20%.

5.5.2 Filter Coefficients: Impulse Response and Transfer Function

The impulse response is generally a short-duration time-domain signal.

A system's impulse response is defined as the output signal that results when an impulse is applied to the system input.

A transfer function is a mathematical relationship between the numerical input to a dynamic system and the resulting output.

In this work it will be estimated the impulsive response and transfer function for the different number of taps and bandwidth margins for two way antenna.

Single polarization, bandwidth margin 10% and $PRF = 2700\ Hz$ in the near range:

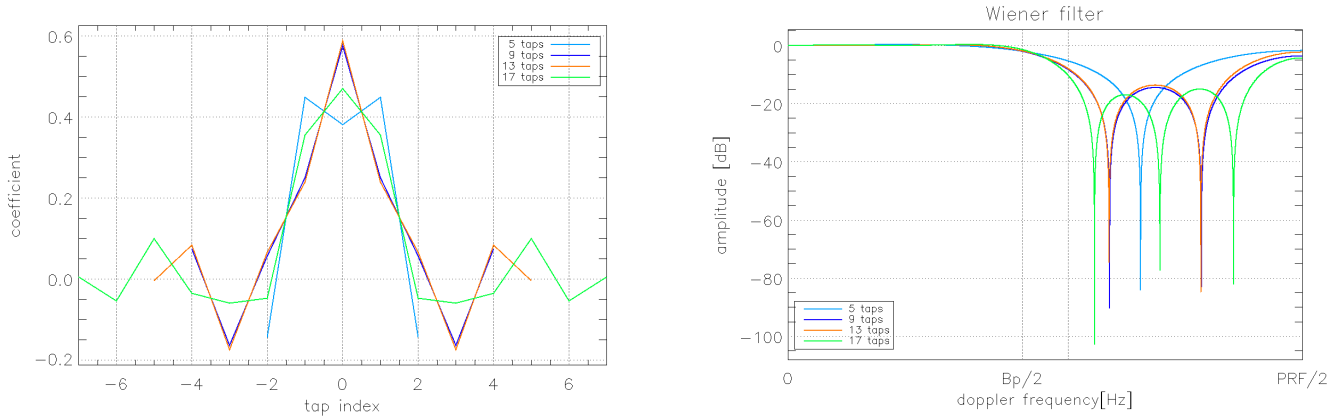

Fig. 31 Impulse Response vs tap index (left)(a) and transfer function vs Doppler frequency (right)(b), for different numbers of taps and bandwidth margin 10% and Transfer function vs Doppler frequency (right) PRF_mean=2700 Hz.

Tab.9 Filter characterization for margin 10% and PRF mean =2700 Hz in single-pol.

Numbers of taps	**Numbers of taps filter**	**Value in dB at PBW/2**
5	5	-2.0295279
9	9	-2.0415432
13	11	-1.9264775
17	15	-1.4563250

The number of taps filter for bw margin 10%, is smaller than the number of taps because PRF resampling is proportional to PRF output, and PRF output is proportional to bandwidth margin and PBW (processed Doppler bandwidth).

$$PRF_{res} = decimation\ factor * PRF_{out} \tag{42}$$

$$PRF_{out} = bw_{margin} * PBW \tag{43}$$

The value at PBW/2 increases with the number of taps. The smaller value of PBW/2 has preferred for its near value to flat response in the processed Doppler bandwidth.

Quad polarization, bandwidth margin 10% and $PRF = 2 * 2000\ Hz$:

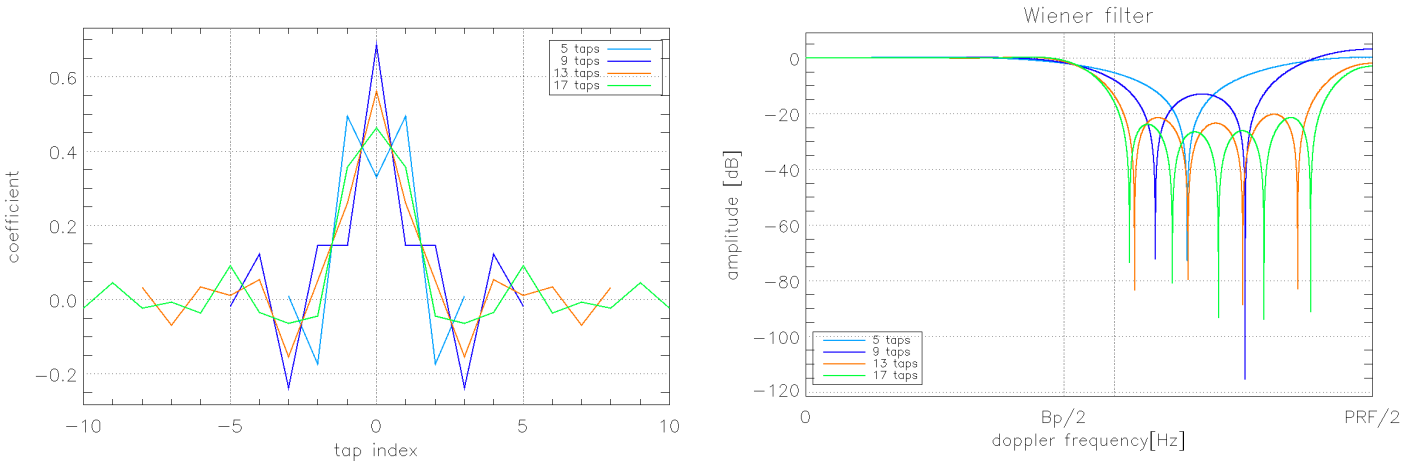

*Fig. 32 Impulse response vs tap index (left)(a), and transfer function vs Doppler frequency (right)(b) for different numbers of taps, bandwidth margin 10% and PRF_mean=2*2000 Hz.*

*Tab.10 Filter characterization for margin 10% and PRF mean =2*2000 Hz in quad-pol.*

Numbers of taps	**Numbers of taps filter**	**Value in dB at PBW/2**
5	7	-1.9264845
9	11	-1.7347372
13	17	-1.2995366
17	21	-0.94265343

Single polarization, bandwidth margin 20% and $PRF = 2700\,Hz$:

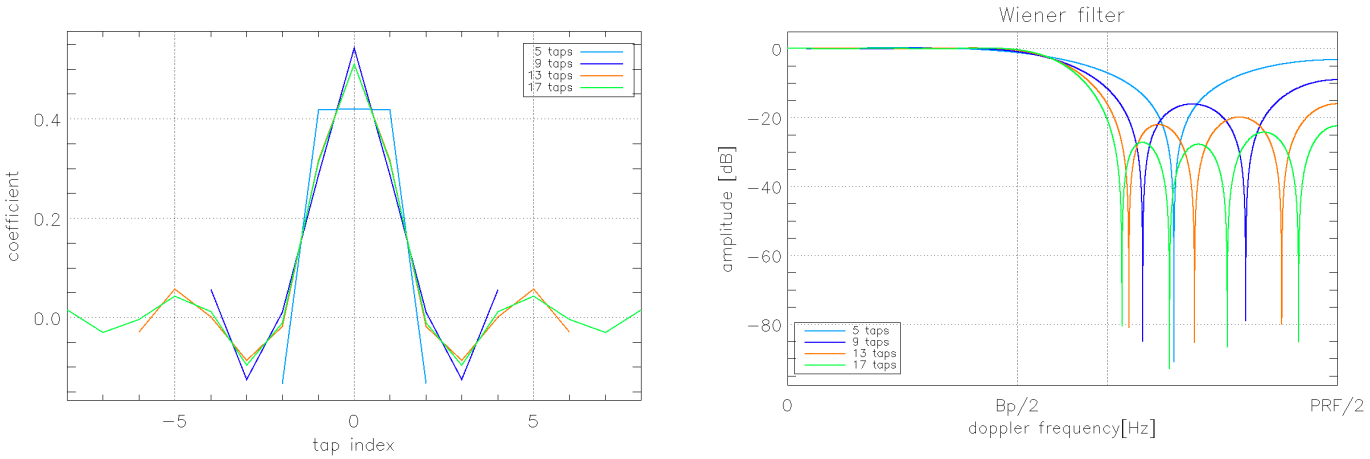

Fig. 33 Impulse response vs tap index (left)(a) and Transfer function vs Doppler frequency (right) (b) for different numbers of taps and bandwidth margin 20%. PRF_mean=2700Hz

Tab.11 Filter characterization for margin 20% and PRF mean =2700 Hz in single-pol

Numbers of taps	Numbers of taps filter	Value in dB at PBW/2
5	5	-1.1869005
9	9	-0.93777123
13	13	-0.54087098
17	17	-0.35519593

Quad polarization, bandwidth margin 20% and $PRF = 2 * 2000\,Hz$:

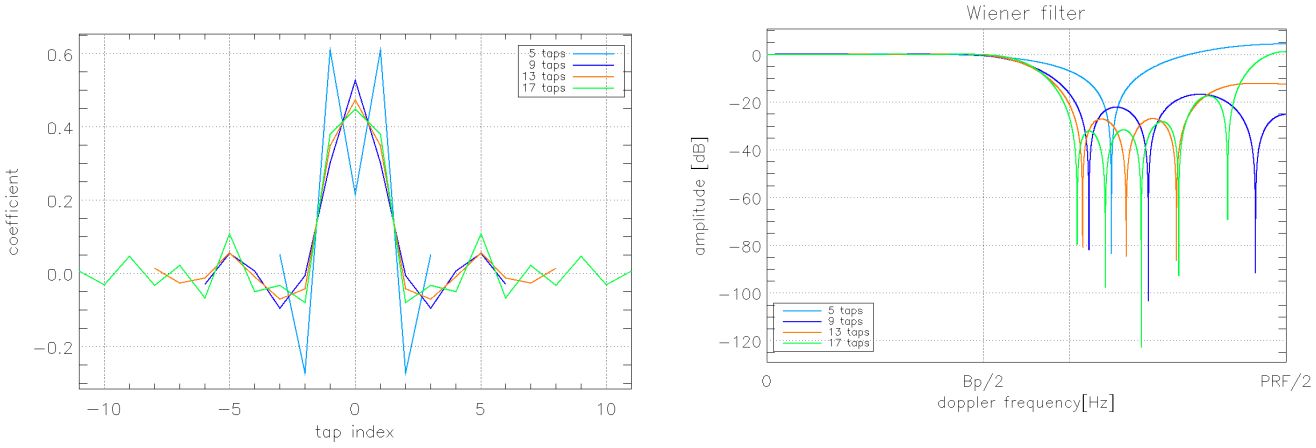

*Fig. 34 Impulse response vs tap index (left)(a) and Transfer function vs Doppler frequency (right) (b) for different numbers of taps and bandwidth margin 20%. PRF_mean=2*2000 Hz.*

*Tab. 12 Filter characterization for margin 20% and PRF mean =2*2000 Hz in quad-pol.*

Numbers of taps	Numbers of taps filter	Value in dB at PBW/2
5	7	-0.64543079
9	13	-0.52878187
13	17	-0.34239001
17	23	-0.10313535

Single polarization, bandwidth margin 30% and $PRF = 2700\ Hz$:

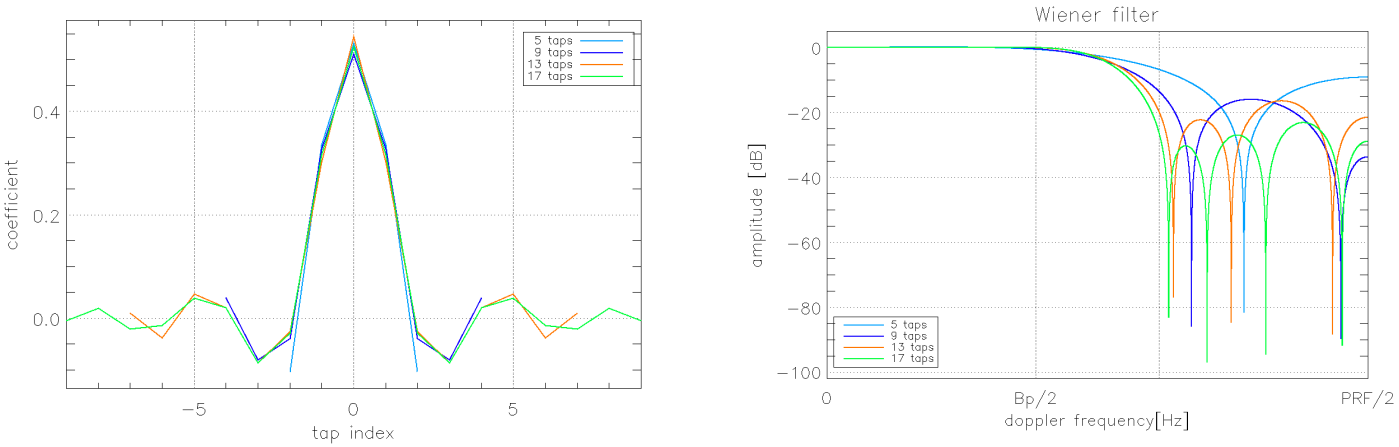

Fig. 35 Impulse response vs tap index (left)(a) and Transfer function vs Doppler frequency (right) (b) for different numbers of taps and bandwidth margin 30%. PRF_mean=2700 Hz.

Tab. 13 Filter characterization for margin 30% and PRF mean =2700 Hz in single-pol.

Numbers of taps	Numbers of taps filter	Value in dB at PBW/2
5	5	-0.65180491
9	9	-0.44880895
13	15	-0.095660733
17	19	-0.048286796

Quad polarization, bandwidth margin 30% and $PRF = 2 * 2000\,Hz$:

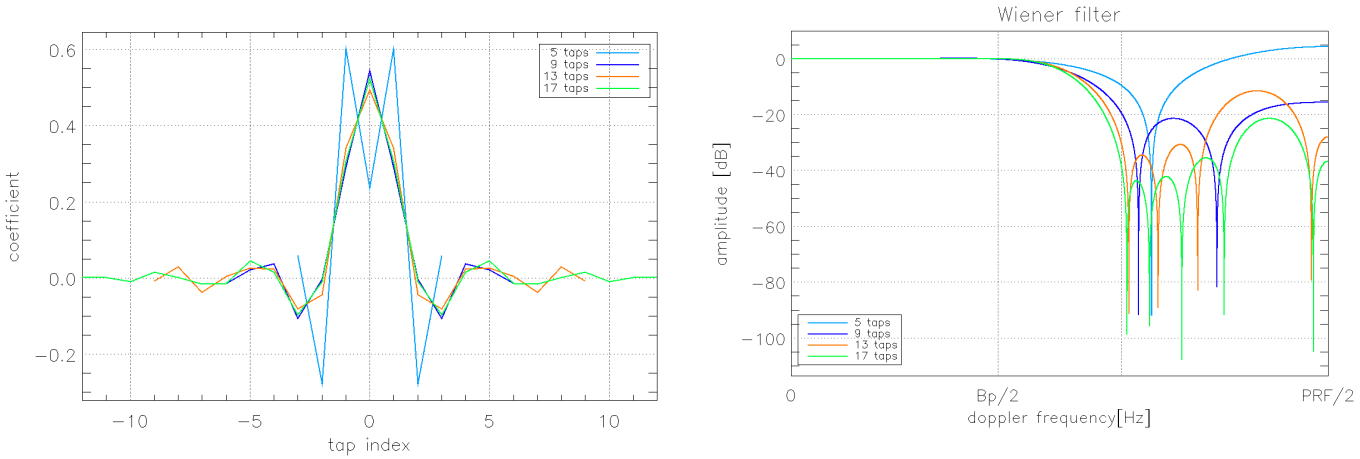

*Fig. 36 Impulse response vs tap index (left)(a) and Transfer function vs Doppler frequency (right) (b) for different numbers of taps and bandwidth margin 30%. PRF_mean=2*2000Hz.*

*Tab. 14 Filter characterization for margin 30% and PRF mean =2*2000 Hz in quad-pol.*

Numbers of taps	**Numbers of taps filter**	**Value in dB at PBW/2**
5	7	-0.23921107
9	13	-0.18853776
13	19	-0.033457702
17	25	-0.021131721

In Quad-pol fig. 32, 34, 36 and tabs 10,14 are displayed more taps than in impulse response, because for a small PRF corresponds a major number of filter taps, while for a high PRF corresponds a minor number of filter taps. In single-pol increasing the bandwidth margin the sidelobe decreases, in fact compared to 10% fig 31 (a), the graphs 33a and 35a, that are related to 20% and 30% have smaller sidelobes. In quad-pol increasing the bandwidth margin, the sidelobes for 5 taps increase while 9,13,17 decrease as shown in fig. 32a, 34a, 36a.

In the case of transfer function the PRF resampling increases with bandwidth margin. The value at PBW/2 increases with the bandwidth margin. In the case of 30% of bandwidth margin, fig. 35b, 36b the PBW/2 is near to flat response, in particular for quad-pol the values are near to zero. The acceptable values, of the transfer function, are those for which amplitude of the secondary lobes is lower than the mainlobe. The fig. 31b, relative to transfer function for single polarization and bandwidth margin 10%, shows the acceptable value is 17 taps. The fig. 32b, relative to transfer function for quad polarization and bandwidth margin 10%, shows that the acceptable curves are

13 and 17 taps. The fig. 33b, relative to transfer function for single polarization and bandwidth margin 20%, shows that only 5 taps are not acceptable. The fig. 34b, relative to transfer function for quad polarization and bandwidth margin 20%, shows that the acceptable value are 9 and 13 taps. The fig. 35b, relative to transfer function for single polarization and bandwidth margin 30%, shows that all taps are acceptable. The fig. 36b, relative to transfer function for single polarization and bandwidth margin 30%, shows that only 5 taps are not acceptable.

6 Conclusions

This thesis analyzes a suboptimal algorithm for data volume reduction in Staggered SAR systems subject to limited onboard memory. This chapter concludes the thesis with an overview of the achieved results and an outlook on further research.

6.1 Thesis Objectives and Results

The SAR sensors have become an essential part of current Earth observation systems, because they are able to provide high resolution imaging in all-weather, day and night coverage of the earth's surface. SAR could give virtually continuous observation of the Earth, simplifying the monitoring of dynamic processes.

In recent years, more SAR complexes have developed, surpassing conventional SARs. The new generation of HRWS SAR overcomes the limit of traditional SAR and permits to have at the same time high resolution and wide swath. In a few days it is possible to obtain continuous global coverage. Moreover, using technologies like Staggered SAR is possible to remove "blind ranges" between subswaths varying the locations of the blind ranges from pulse to pulse. The missing sample in raw data causes additional ambiguous energy in the focused SAR image. For these reasons PRIs should be designed such that two consecutive azimuth samples are never missed and should be done an oversampling in azimuth. Thanks to the BLU interpolation is possible to recover uniformly sampled data from non-uniform raw data. While with FIR filter is possible to remove part of ambiguous energy, reduce interference, and noise in Fourier transform data.

All these aspects contribute to increase the data volume on board satellite, making the downlink difficult and incurring the FPGA's limited memory. The core of this thesis is to reduce the data volume on board processing. There are a lot of advantages to make on-board processing like reducing the amount of raw data to be stored, reduce the number ground station, fewer data to transmit to the ground station and improve the downlink.

This thesis analyzes a suboptimal algorithm that selects in the input only a limited number of taps of raw data and meets the limited memory of the FPGA. The selected taps of raw data include missing samples. The BLU interpolation permits to recover uniformly grid sampled data. The taps of raw data and the taps of resampled data are selected around the output tap. Applying the Doppler filter to the resampled data is possible to obtain the output tap which composes the

filtered data. Repeating this procedure shifting along azimuth and selected again a new sequence of taps from raw data, is possible to obtain a complete sequence of filtered data. The data in output will have a reduced PRF with a consequent reduction in data volume.

The question to be answered was how much that algorithm degraded the performance of Staggered SAR. Different parameters were examined like AASR, AASR degradation, PSLR, azimuth resolution and filter coefficients. A comparison was made with these parameters between Staggered SAR on board processing with limited numbers of taps and Staggered SAR on board processing considering all taps. Furthermore, different numbers of taps and different bandwidth margin for single and quad polarization, were considered.

In this thesis were selected 5,9,13,17 numbers of taps for the simulations. The working bandwidth margin is 20% and 30%. The results show for single and quad polarization that for 30% bandwidth the taps 9,13,17 are better than 20%, and the opposite for 5 taps. The PSLR is better for 20% of the bandwidth for 5,13,17 taps, while for 9 taps is better 30% of bandwidth margin. The resolution in azimuth does not particularly degrade changing the bandwidth margin. In this thesis it was also evaluated the impulse response and transfer function for 20% and 30% bandwidth margin for single and quad polarization. In quad polarization are displayed more taps in the impulse response, this happens because for a small PRF corresponds a major number of filter taps, while for a high PRF corresponds a minor number of filter taps. Increasing the bandwidth margin the sidelobe decreases. The PRF resampling increases with bandwidth margin. For 30% of bandwidth margin the PBW/2 is near to flat response, in particular for quad-pol the values are near to zero.

Ultimately, it is possible to affirm that major value of bandwidth margin, like 30% is better for AASR and PSLR considering not too much small numbers of taps, moreover there are others benefits like PBW/2 is near to flat response and sidelobe decreases. A major value of bandwidth at the same time means more data in downlink, this means that is needed the right compromise based on the chosen mission.

Bibliography

[1] Credit: DLR; date: July 8, 2007; https://www.dlr.de/dlr/en/desktopdefault.aspx/tabid-10680/#gallery/5078

[2] Michael Eineder, Irena Hajnsek, Gerhard Krieger, Alberto Moriera, Kostas Papathanassiou, "Tandem L: Satellite Mission Proposal for Monitoring Dynamic Processes on the Earth's Surface", German Aerospace Center (DLR), Cologne, 2018.

[3] Credit: DLR; https://www.dlr.de/hr/en/desktopdefault.aspx/tabid-8113/14171_read-35837/

[4] M. Villano, "Staggered Synthetic Aperture Radar", Ph.D. dissertation, Institute of Radio Frequency Engineering and Electronics (IHE), Karlsruhe Institute of Technology (KIT), Karlsruhe, Germany, February 2016.

[5] A. Moreira, P. Prats-Iraola, M. Younis, G. Krieger, I. Hajnsek and K. P. Papathanassiou, "A Tutorial on Synthetic Aperture Radar", in IEEE Geoscience and Remote Sensing Magazine, vol. 1, no. 1, pp. 6-43, March 2013.

[6] M. Villano, G. Krieger, A. Moreira, "Reconsideration of Ambiguities in Quad-Pol SAR", EUSAR 2016.

[7] G. Krieger, S. Huber, M. Younis, A. Moreira, J. Reimann, P. Klenk, M. Zink, M. Villano, F. Queiroz de Almeida "In-Orbit Relative Amplitude and Phase Antenna Pattern Calibration for Tandem-L" in EUSAR 2018.

[8] G. Krieger, M. Younis, N. Gebert, S. Huber, F. Bordoni, A. Patyuchenko, A. Moreira, "Advanced Concepts for Ultra-Wide-Swath SAR Imaging" Proceedings of the EUSAR, Friedrichshafen, Germany, 2008.

[9] M. Villano, G. Krieger and A. Moreira, "Staggered SAR: High-Resolution Wide-Swath Imaging by Continuous PRI Variation", in IEEE Transactions on Geoscience and Remote Sensing, vol. 52, no.7, pp. 4462-4479, 2014.

[10] Nicolas Gebert, Gerhard Krieger, Alberto Moriera, “Digital Beamforming on Receive: Techniques and Optimization Strategies for High-Resolution Wide-Swath” in IEEE on transactions on Aerospace and Electronic Systems vol. 45, no. 2, april 2009.

[11] Laurens Bierens, Rob van Heijster, Hans van Bezouwen “Data Reduction using Real-Time On Board Satellite SAR Processing” in TNO Physics and Electronics Laboratory, Netherlands.

[12] Martin Suess, Christoph Schaefer and Rolf Zahn, “The Technology Development of a Spaceborne On-Board SAR-Processor and Storage Demonstrator”, Dornier Satellite Systems, Friedrichshafen, Germany.

[13] Thomas Kailath, “A View of Three Decades of Linear Filtering Theory”, IEEE transactions on information theory, vol. it-20, no.2, March 1974.

[14] I. Hajnsek, M. Shimada, M. Eineder, K. P. Papathanassiou, T. Motohka, M. Watanabe, M. Ohki, F. de Zan, F. Lopez-Dekker, G. Kieger, and A. Moriera “Tandem-L: Science requirements and mission concept”, Proceedings of the EUSAR, Berlin, Germany, 2014.

[15] P. Berens, “Introduction to Synthetic Aperture Radar (SAR)”, Research Institute for High-Frequency Physics and Radar Techniques (FHR), Research Establishment for Applied Science (FGAN), Wachtberg, Germany.

[16] Wiener, “The interpolation, extrapolation and smoothing of stationary time series”, Report of the Services 19, Research Project DIC-6037 MIT, February 1942.

[17] Wiener, Norbert, “Extrapolation, Interpolation, and Smoothing of Stationary Time Series”, New York: Wiley,1949.

[18] A. Moreira, G. Krieger, I. Hajnsek, K. Papathanassiou, M. Younis, P. Lopez-Dekker, S. Huber, M. Villano, M. Pardini, M. Eineder, F. De Zan, A. Parizzi, “Tandem-L: A Highly Innovative Bistatic SAR Mission for Global Observation of Dynamic Processes on the Earth's Surface,” IEEE Geoscience and Remote Sensing Magazine, vol. 3, no. 2, pp. 8-23, June 2015.

[19] M. Villano, G. Krieger, M. Jäger, A. Moreira, “Staggered SAR: Performance Analysis and Experiments with Real Data,” IEEE Transactions on Geoscience and Remote Sensing, vol. 55, no. 11, pp. 6617-6638, Nov. 2017.

[20] S. Huber, A. Patyuchenko, G. Krieger and A. Moreira, “Spaceborne Reflector SAR Systems With Digital Beamforming”, in IEEE Transactions on Aerospace and Electronic Systems, vol. 48, no. 4, pp.3473-3493, 2012.